

14-3-3 ζ allows for adipogenesis by modulating chromatin accessibility during the early stages of adipocyte differentiation



Sabri A. Rial^{1,2,**}, Zhipeng You³, Alexis Vivoli^{1,2}, Frédéric Paré², Daphné Sean^{1,2}, Amal AlKhoury^{1,2}, Geneviève Lavoie^{4,5}, Mete Civelek^{6,7}, Aida Martinez-Sanchez⁸, Philippe P. Roux^{4,5}, Thomas M. Durcan³, Gareth E. Lim^{1,2,*}

ABSTRACT

Objective: We previously established the scaffold protein 14-3-3 ζ as a critical regulator of adipogenesis and adiposity, but whether 14-3-3 ζ exerted its regulatory functions in mature adipocytes or in adipose progenitor cells (APCs) remained unclear.

Methods: To decipher which cell type accounted for 14-3-3 ζ -regulated adiposity, adipocyte- (*Adipoq*14-3-3 ζ KO) and APC-specific (*Pdgfra*14-3-3 ζ KO) 14-3-3 ζ knockout mice were generated. To further understand how 14-3-3 ζ regulates adipogenesis, Tandem Affinity Purification (TAP)-tagged 14-3-3 ζ -expressing 3T3-L1 preadipocytes (TAP-3T3-L1) were generated with CRISPR-Cas9, and affinity proteomics was used to examine how the nuclear 14-3-3 ζ interactome changes during the initial stages of adipogenesis. ATAC-seq was used to determine how 14-3-3 ζ depletion modulates chromatin accessibility during differentiation.

Results: We show a pivotal role for 14-3-3 ζ in APC differentiation, whereby male and female *Pdgfra*14-3-3 ζ KO mice displayed impaired or potentiated weight gain, respectively, as well as fat mass. Proteomics revealed that regulators of chromatin remodeling, like DNA methyltransferase 1 (DNMT1) and histone deacetylase 1 (HDAC1), were significantly enriched in the nuclear 14-3-3 ζ interactome and their activities were impacted upon 14-3-3 ζ depletion. Enhancing DNMT activity with S-Adenosyl methionine rescued the differentiation of 14-3-3 ζ -depleted 3T3-L1 cells. ATAC-seq revealed that 14-3-3 ζ depletion impacted the accessibility of up to 1,244 chromatin regions corresponding in part to adipogenic genes, promoters, and enhancers during the initial stages of adipogenesis. Finally, 14-3-3 ζ -regulated chromatin accessibility correlated with the expression of key adipogenic genes.

Conclusion: Our study establishes 14-3-3 ζ as a crucial epigenetic regulator of adipogenesis and highlights the usefulness of deciphering the nuclear 14-3-3 ζ interactome to identify novel pro-adipogenic factors and pathways.

© 2025 The Author(s). Published by Elsevier GmbH. This is an open access article under the CC BY-NC license (<http://creativecommons.org/licenses/by-nc/4.0/>).

Keywords 14-3-3 ζ ; Adipogenesis; Energy homeostasis; Chromatin accessibility; Adipogenic genes; Epigenetic regulation

1. INTRODUCTION

The expansion of adipocyte number occurs through adipocyte differentiation, or adipogenesis, and this process plays a pivotal role in the development of obesity [1–3]. The differentiation of adipose progenitor cells (APCs) is driven by the availability of energy-dense nutrients and a variety of adipogenic triggers, and adipogenesis is facilitated by complex signaling pathways and tightly regulated transcriptional networks [4,5].

The canonical model of adipogenesis posits that hormonal and nutrient stimuli promote the sequential expression and activation of early

adipogenic transcription factors (ATFs), which include CCAAT-enhancer-binding proteins- β/δ (C/EBP- β/δ), STAT5A signal transducer and activator of transcription 5A/B (STAT5A/B), Kruppel-like factor 5 (KLF5), and glucocorticoid receptor (GR) and late ATFs, such as C/EBP α and Peroxisome proliferator-activated receptor γ 2 (PPAR γ 2) [4,5]. Although these events take place during the early stages of APC differentiation, little is known about the molecular factors that tightly coordinate them in space (*i.e.*, cytosolic to nuclei translocation) and time (sequential activation of ATFs). This lack of knowledge has contributed to the difficulty in targeting adipogenesis with pharmacological approaches to treat obesity.

¹Department of Medicine, Université de Montréal, Montreal, QC, Canada ²Cardiometabolic Axis, Centre de Recherche du Centre Hospitalier de l'Université de Montréal (CRCHUM), Montréal, QC, Canada ³The Neuro's Early Drug Discovery Unit (EDDU), McGill University, 3801 University Street, Montreal, QC, H3A 2B4, Canada ⁴Institute for Research in Immunology and Cancer (IRIC), Université de Montréal, Montréal, QC, Canada ⁵Department of Pathology and Cell Biology, Faculty of Medicine, Université de Montréal, Montréal, QC, Canada ⁶Department of Biomedical Engineering, University of Virginia, Charlottesville, United States ⁷Center for Public Health Genomics, University of Virginia, Charlottesville, VA, 22908, United States ⁸Section of Cell Biology and Functional Genomics, Department of Metabolism, Digestion and Reproduction, Imperial College London, Hammersmith Hospital, London, UK

**Corresponding author. CRCHUM, Tour Viger, Rm 08.734, Rue St. Denis, Montréal, QC, H2X 029, Canada. E-mail: ahmed.sabri.rial@umontreal.ca (S.A. Rial).

*Corresponding author. CRCHUM, Tour Viger, Rm 08.482, 900 Rue St. Denis, Montréal, QC, H2X 029, Canada. E-mail: gareth.lim@umontreal.ca (G.E. Lim).

Received March 26, 2025 • Revision received April 17, 2025 • Accepted April 23, 2025 • Available online 28 April 2025

<https://doi.org/10.1016/j.molmet.2025.102159>

Molecular scaffold proteins likely play important roles in coordinating signaling pathways that control metabolism [6,7], and of the various families of scaffolds, the importance of 14-3-3 proteins in signal transduction has become apparent [6,7]. Through recognition of specific phosphorylated serine or threonine motifs (RSXpS/TXP and RXXpS/TXP), all seven mammalian 14-3-3 protein isoforms interact with a broad variety of enzymes, transcription factors, and transporters. Thus, 14-3-3 proteins can regulate diverse cellular processes, such as cell cycle progression, apoptosis, secretion, and metabolism [7,8].

Despite a high degree of sequence-homology, 14-3-3 family members can perform isoform-specific biological functions, and our group has identified critical roles of the 14-3-3 ζ isoform in the regulation of whole-body adiposity, adipogenesis, adipocyte function, and glucose and lipid homeostasis [7,8]. In the context of adipocyte differentiation *in vitro*, silencing of *Ywhaz* (the gene coding for 14-3-3 ζ) blocked the differentiation of 3T3-L1 preadipocytes [9]. We also found that systemic deletion of 14-3-3 ζ significantly reduced visceral adiposity and promoted glucose intolerance and insulin resistance in male mice [9]. Postnatal depletion of 14-3-3 ζ in mature adipocytes was found to reduce adipose tissue *Pparg2* mRNA expression and impair the lipolytic response of adipose tissue [10]. In contrast, whole-body transgenic overexpression of 14-3-3 ζ potentiated age-dependent and high-fat diet-induced expansion of adipose tissue [9]. Taken together, these findings demonstrate important roles of 14-3-3 ζ in adipocyte development and function.

With the ability of 14-3-3 proteins to interact with a diverse array of phosphorylated proteins, we have discovered that the interactome of 14-3-3 ζ changes in response to physiological and pathophysiological stimuli like adipocyte differentiation or obesity, respectively. We first used mouse embryonic fibroblasts derived from transgenic mice expressing a tandem affinity purification (TAP) epitope-tagged 14-3-3 ζ molecule combined with affinity proteomics to discover that the interactome of TAP-14-3-3 ζ is enriched with RNA splicing factors following the induction of adipocyte differentiation [11]. Recently, we have determined that the interactome of 14-3-3 ζ in adipose tissue is also sensitive to high-fat diet-induced obesity [12]. Altogether, these findings demonstrate the usefulness of determining the 14-3-3 ζ interactome in identifying novel regulators of adipocyte differentiation or expansion of adipose tissue mass.

A major limitation of whole-body deletion or overexpression 14-3-3 ζ mouse models is the inability to distinguish the individual contributions of specific cell types, and with our findings that 14-3-3 ζ may regulate adiposity [9,10], whether 14-3-3 ζ primarily influences mature adipocytes or APCs, let alone other cell types, is unclear. Moreover, the recent discovery of adipocyte and APC heterogeneity further adds to the complexity in understanding the roles of specific proteins in adipose tissue niches. Indeed, adipocytes derived from APCs that express different markers such as Platelet-derived growth factor receptor (PDGFR)- α and - β , represent unique sub-populations that can be influenced by age, anatomical localization and nutritional contexts [13–18]. For example, subsets of PDGFR α + cells with high or low expression of CD9 were found to be committed to pro-fibrotic and adipogenic cells, respectively [14]. Also, CD24+ progenitors, and not CD24⁻, were characterized as having high adipogenic potential [15]. The concept of heterogeneity is not restricted to rodents, as spatial technologies have revealed heterogeneity within human adipose tissues [13]. Although systemic 14-3-3 ζ deletion and over-expression had opposing effects on adiposity, it is not clear whether 14-3-3 ζ is differentially expressed in APCs or mature adipocytes to account for the differences in fat mass.

Herein, we sought to examine the impact of deleting 14-3-3 ζ in *Adipoq*+ mature adipocytes (*Adipoq*14-3-3 ζ KO) and in *Pdgfra*+ APCs (*Pdgfra*14-3-3 ζ KO) on murine adiposity under normal chow and high-fat diet conditions. No differences in body weights were found in *Adipoq*14-3-3 ζ KO mice. However, *Pdgfra*14-3-3 ζ KO male mice showed moderate reduction in body weight while *Pdgfra*14-3-3 ζ KO female mice exhibited marked increases in body weight, adiposity and fat mass. These observations suggest critical roles of 14-3-3 ζ in APCs rather than in mature adipocytes. To further define processes regulated by 14-3-3 ζ in the differentiation of APCs, CRISPR-Cas9 genome editing was used to generate 3T3-L1 preadipocytes that express a TAP-tagged 14-3-3 ζ molecule to permit the identification of the nuclear interactome of 14-3-3 ζ during the early stages of adipogenesis. Chromatin remodeling was among the highest enriched biological functions, which led to the use of Assay for Transposase-Accessible Chromatin with sequencing (ATAC-seq) to assess how 14-3-3 ζ influences chromatin accessibility. We found that the expression of critical adipogenic genes, such as *Fabp4*, *Adig*, *Retn*, and *Fam83a*, are correlated with 14-3-3 ζ -regulated chromatin accessibility. Taken together, our study highlights the importance of 14-3-3 ζ during the early stages of adipogenesis and a novel role by which it regulates adipocyte differentiation.

2. RESULTS

2.1. Adipose expression of *Ywhaz* correlates with body fat mass and insulin resistance in mice

With the finding that extreme differences in *Ywhaz* expression are associated with opposite effects on adiposity [9], we first wanted to determine if natural variations in *Ywhaz* mRNA expression are similarly correlated with adiposity and other metabolic parameters. Thus, the Hybrid Mouse Diversity Panel (HMDP) was used to explore the association of *Ywhaz* mRNA expression in perigonadal adipose tissue samples with metabolic traits. The HMDP is composed of one hundred inbred strains of male and female mice that were fed a high-fat and high-sugar (HF/HS) diet for 8 weeks and assessed for metabolic parameters such as body weight, lean and fat masses, fasting glycemia, and insulinemia [19]. A significantly positive correlation between *Ywhaz* expression and insulin resistance, as measured by HOMA-IR, was detected in male and female mice after HF/HS feeding (bico >0.4 , $P < 10^{-9}$, Figure 1A,D). Percent fat mass before and after HF/HS diet feeding in males (Figure 1B,C) and females (Figure 1E,F) were also found to be significantly correlated with *Ywhaz* mRNA expression. To better understand the contribution of 14-3-3 ζ to adipogenesis, we assessed how siRNA-mediated knockdown of *Ywhaz* would impact the differentiation of 3T3-L1 preadipocytes treated with established adipogenic cocktails of Insulin, Dexamethasone, and IBMX (MDI) and MDI with Rosiglitazone (MDIR) [9,10] (Figure 1G). Depletion with si*Ywhaz* suppressed 3T3-L1 differentiation, as confirmed by significantly reduced Oil Red-O staining (Figure 1H,I) and significantly attenuated expression of *Pparg2* and *Adipoq* mRNAs (Figure 1J,K). In siCTL-transfected cells, expression of *Ywhaz* reached maximal levels by day 2 of differentiation with MDIR, and by Day 8 with MDI (Figure 1L). These results replicated the effects of si*Ywhaz* on adipogenesis that we published previously [9].

Altogether, these observations establish a positive association between adipose tissue expression of *Ywhaz* and adiposity, and confirm the requirement of *Ywhaz* for the differentiation of fibroblasts into adipocytes.

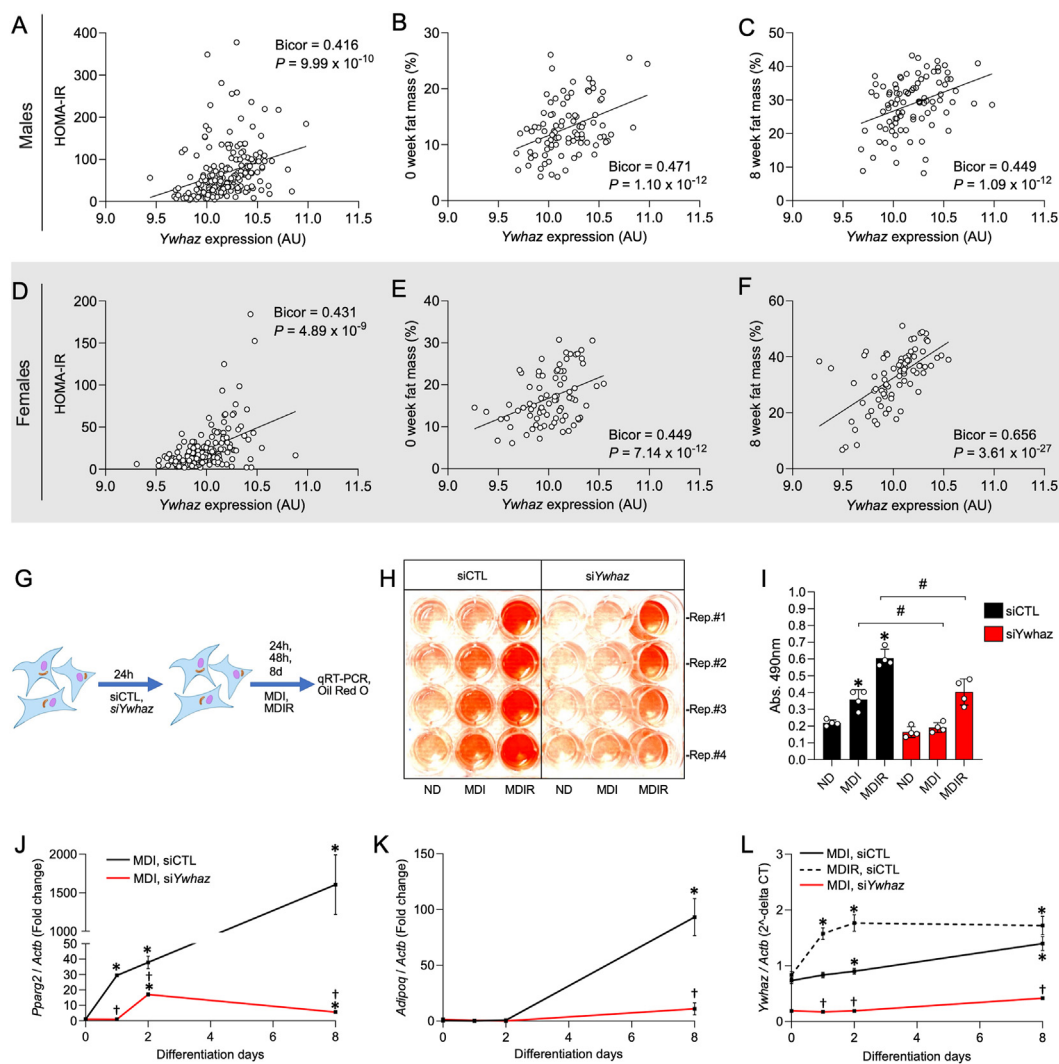


Figure 1: Adipose tissue expression of *Ywhaz* is positively correlated with body fat mass and insulin resistance in male and female mice. Correlation of (A–C) male and (D–F) female perigonadal adipose tissue (VAT) gene expression of *Ywhaz* with HOMA-IR (A and D) and whole body fat mass before (B and E) and after (C and F) high-fat, high-sucrose feeding, using the Hybrid Mouse Diversity Panel (HMDP) resource [19]. (G) Timeline of the experiment performed on 3T3-L1 cells transfected with siCTL or siYwhaz (10 nM each) prior to standard MDI or MDIR differentiation protocols [9,10,87]. After treatments, cells were subjected to Oil Red-O staining (H), measurement of Oil Red-O incorporation level by absorbance at 490 nm (I), and qRT-PCR to measure *Pparg2* (J), *Adipoq* (K) and *Ywhaz* (L) mRNA levels. Significant differences between experimental conditions are indicated by * $P < 0.05$ or # $P < 0.05$ (calculated by Student's t-test). (For interpretation of the references to color in this figure legend, the reader is referred to the Web version of this article.)

2.2. Deletion of 14-3-3 ζ in mature adipocytes does not impact adiposity in chow-fed mice

To determine if deletion of 14-3-3 ζ in mature white adipocytes affects postnatal adiposity, we bred *Adipoq*^{EVDR}-Cre transgenic mice [20] with *Ywhaz*^{fllox/fllox} mice [10,21] to generate mature adipocyte-specific 14-3-3 ζ knockout mice (*Adipoq*14-3-3 ζ KO). Our aim was to assess how adipocyte-specific 14-3-3 ζ deletion affects adiposity and metabolic homeostasis in chow-fed mice. We confirmed by quantitative PCR that *Ywhaz* expression was nearly abolished in mature white adipocytes, but not in the stromal vascular fraction (SVF) of adipose tissues of males and female KO mice (Figure 2A,K; Sup. Fig. 1A,B). In male mice, mRNA levels of some 14-3-3 isoforms, namely *Ywhae*, *Ywhag*, and *Ywhah*, were significantly increased, but these increases were not seen in females (Sup. Fig. 1C,D). Deletion of 14-3-3 ζ in mature

adipocytes resulted in mild and significant perturbations in glucose tolerance in male and female mice, respectively (Figure 2C,M); however, no differences in insulin sensitivity were detected in both sexes (Figure 2D,N).

Compared to WT controls, male or female *Adipoq*14-3-3 ζ KO mice showed no differences in body weight gain (Figure 2B,L), perigonadal and inguinal adipocyte size (Figure 2E–G, O–Q), or fat mass (Figure 2H–J, R–T). Similarly, no changes in the expression of key metabolic genes, namely *Srebf1*, *Hsl*, *Atgl*, *Slc2a4*, and *Adipoq*, were detected in inguinal and perigonadal adipose tissues of both groups (Sup. Fig. 1E,F). The pro-inflammatory marker, *Tnfa*, was markedly decreased in both fat depots of female *Adipoq*14-3-3 ζ KO mice (Sup. Fig. 1F). Altogether, these observations indicate that, under chow feeding conditions, 14-3-3 ζ does not impact the fate of mature adipocytes.

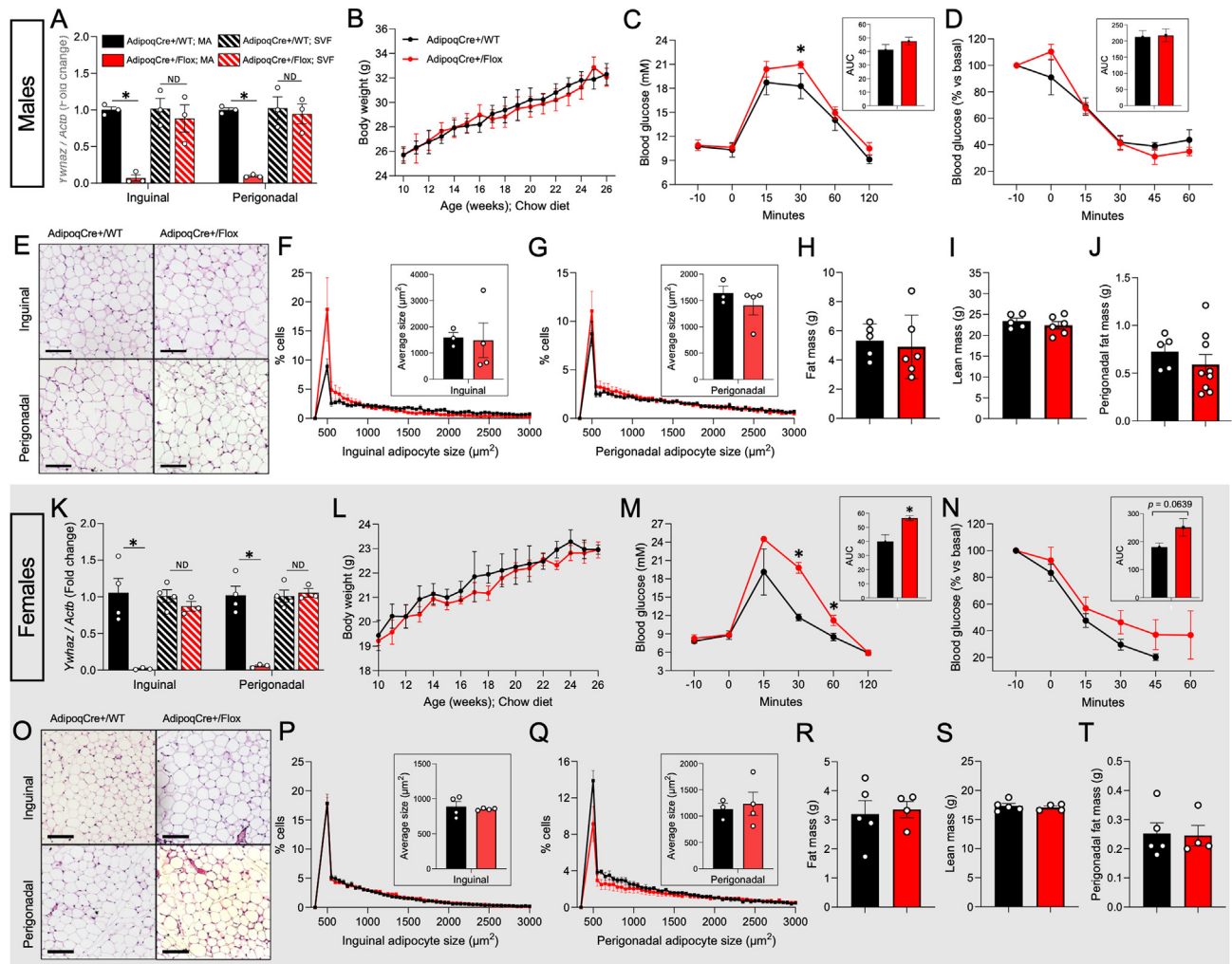


Figure 2: Deletion of 14-3-3 ζ in mature adipocytes does not affect adiposity, but impairs glucose tolerance. (A–J) Male and (K–T) female wild type (*AdipoqCre*+WT) and *Adipoq14-3-3 ζ* KO (*AdipoqCre*+Flox) mice were generated by breeding *Adipoq*-Cre mice with either WT mice or mice harboring floxed alleles of *Ywhaz*. Animals were fed a chow diet exclusively. (A,K) Inguinal (SAT) and perigonadal (VAT) adipose tissue samples were subjected to qRT-PCR to measure *Ywhaz* mRNA levels ($n = 3–4$ per sex per genotype). Mice ($n = 4$ minimum) were followed for (B and L) body weight gain from 10 to 26 weeks of age, assessed for (C, M) glucose tolerance and (D,N) insulin sensitivity via ip-GTT (2 g kg⁻¹ B.W. α -glucose) and ip-ITT (1.0 U kg⁻¹ humulin® R) at 25 and 26 weeks, respectively. (E,O) H&E-stained microsections (scale bar = 200 μ m) from inguinal and perigonadal adipose tissues were analysed for (F,P) white adipocyte area and (G,Q) size distribution with Visiomorph™. (H–J, R–T) Body composition of mice were measured by EchoMRI™ prior to sacrifice. Error bars represent S.E.M. Significant differences between wild type and *Adipoq14-3-3 ζ* KO mice are indicated by * $P < 0.05$ (calculated by Student's t-test).

2.3. Deletion of 14-3-3 ζ in mature adipocytes protects female mice against high-fat diet-induced obesity

We next assessed if deletion of 14-3-3 ζ in mature adipocytes prevents adipose tissue expansion and metabolic impairments in response to high-fat diet (HFD) feeding. In male WT and *Adipoq14-3-3 ζ* KO mice, HFD feeding for 10 weeks resulted in unaltered body weight gain, adiposity, and metabolic features (Sup. Fig. 2A–I). In contrast, we found that HFD-fed female *Adipoq14-3-3 ζ* KO mice had significantly lowered body weight gain (Sup. Fig. 2J), which was associated with significantly decreased perigonadal fat (Sup. Fig. 2K–M) and 25% smaller inguinal and visceral adipocytes (Sup. Fig. 2N, O). Obese *Adipoq14-3-3 ζ* KO female mice also had improved glucose tolerance and insulin sensitivity (Sup. Fig. 2P, Q), as well as lowered hepatic mass (Sup. Fig. 2R). These findings demonstrate that female, but not male, *Adipoq14-3-3 ζ* KO mice are protected against HFD-induced obesity and associated metabolic impairments.

2.4. Deletion of 14-3-3 ζ in adipocyte progenitors of chow-fed mice impacts body weight and adiposity

The lack of effect on adiposity in chow-fed *Adipoq14-3-3 ζ* KO mice seemed conflicting with our previous finding that whole body KO of 14-3-3 ζ significantly reduces visceral adiposity and adipocyte maturity [9]. We therefore hypothesized that 14-3-3 ζ may play critical roles at earlier stages of adipogenesis, and more precisely in APCs. To address this hypothesis, we deleted 14-3-3 ζ in APCs by breeding *Pdgfra*-Cre mice [22] with *Ywhaz*^{flox/flox} to generate *Pdgfra14-3-3 ζ* KO mice. We confirmed in male and female KO mice by quantitative PCR that *Ywhaz* expression was significantly decreased in the SVF, which is known to contain the *Pdgfra*+ APCs [23], and nearly abolished in mature adipocytes, which mostly originate from *Pdgfra*+ APCs [23–25] (Figure 3A, K; Sup. Fig. 3A, B). Of note, mRNA levels of various 14-3-3 isoforms were altered in inguinal or gonadal adipose tissues in male and female KO mice (Sup. Fig. 3C, D).

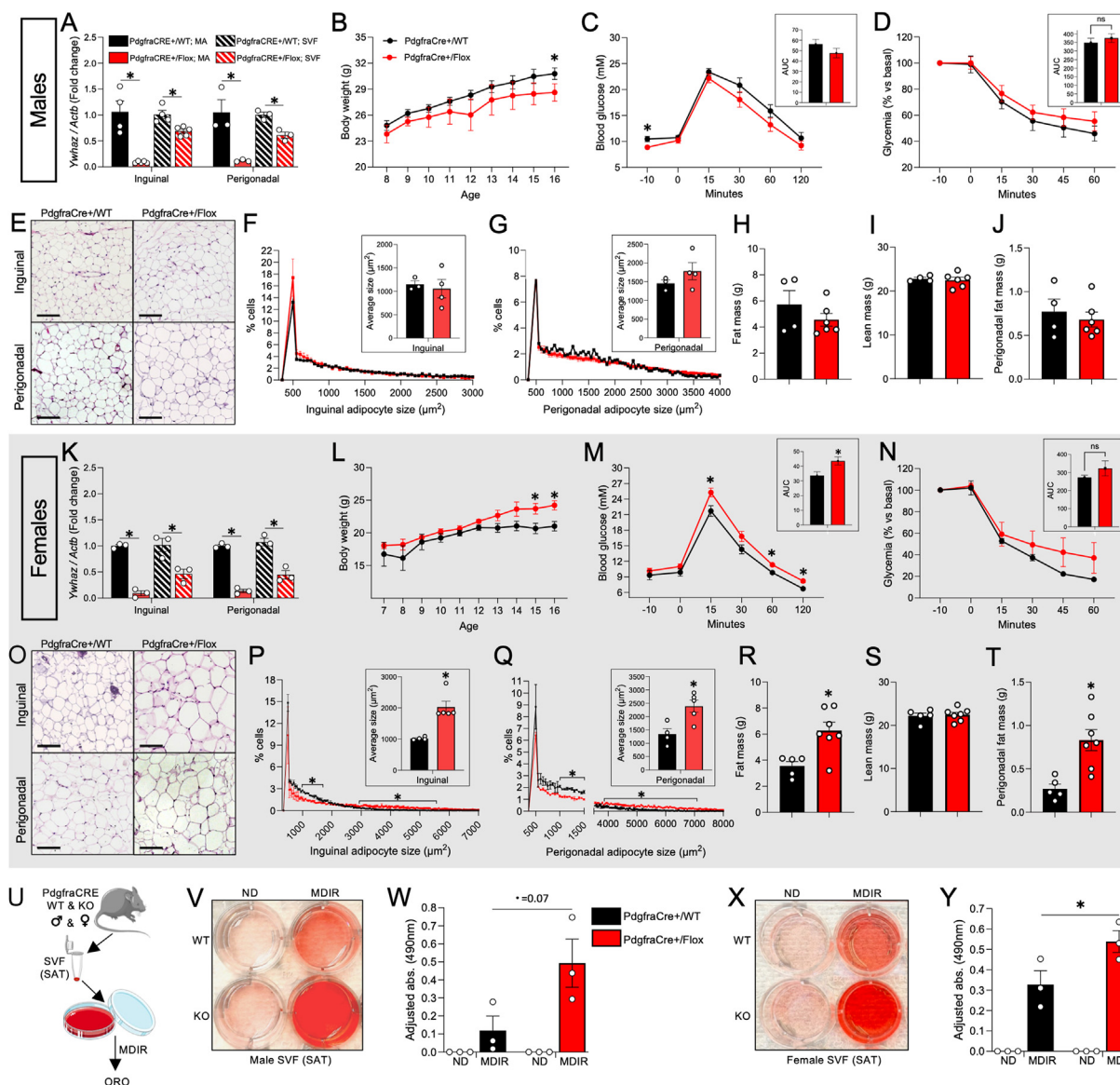


Figure 3: Deletion of 14-3-3 ζ in adipocyte progenitor cells affects adiposity. Male (A–J) and female (K–T) wild type (*Pdgfra*Cre+/WT) and *Pdgfra*14-3-3 ζ KO (*Pdgfra*Cre+/Flox) mice were generated by breeding *Pdgfra*-Cre mice with either WT mice or mice harboring floxed alleles of *Ywhaz* and fed a chow diet. (A,K) Inguinal (SAT) and perigonadal (VAT) adipose tissue samples were subjected to qRT-PCR to measure *Ywhaz* mRNA levels ($n = 3–4$ per sex per genotype). (B,L) Mice ($n = 4$ minimum) were followed for body weight gain from 10 to 26 weeks of age, assessed for (C,M) glucose tolerance and (D, N) insulin sensitivity via ip-GTT (2 g kg⁻¹ B.W. D-glucose) and ip-ITT (1.0 U kg⁻¹ Humulin® R) at 25 and 26 weeks, respectively. (E, O) H&E-stained microsections (scale bar = 200 μ m) from inguinal and perigonadal adipose tissues were analysed for (F, P) white adipocyte area and (G, Q) size distribution with Visiomorph™. (H–J, R–T) Body composition of mice were measured by EchoMRI™ prior to sacrifice. (U) Experimental procedure for the extraction of SVF from subcutaneous white adipose tissues from male (V and W) and female (X and Y) WT mice for plating, culture, and treatment with MDIR, followed by Oil Red-O staining. Differentiated or non-differentiated SVF from male (V and W) and female (X and Y) mice were subjected to Oil Red-O staining (V and Y) and quantification of its accumulation level by absorbance at 490 nm (W and Y). Error bars represent S.E.M. Significant differences between WT and *Pdgfra*14-3-3 ζ KO mice are indicated by * $P < 0.05$ (calculated by Student's *t*-test). (For interpretation of the references to color in this figure legend, the reader is referred to the Web version of this article.)

Compared with WT controls, chow-fed *Pdgfra*14-3-3 ζ KO males exhibited decreased body weight by the experimental endpoint (Figure 3B) and a slight tendency towards decreased adiposity (Figure 3H). No notable effects on glucose tolerance and insulin sensitivity were observed (Figure 3C,D). Deletion of 14-3-3 ζ in APCs of male mice did not significantly affect the expression of key metabolic genes (Sup. Fig. 3E), adipocyte size (Figure 3. E–G), or whole and visceral fat mass (Figure 3H–J).

In contrast, *Pdgfra*14-3-3 ζ KO female mice exhibited significantly increased body weight by 16 weeks of age (Figure 3L), despite being

fed a chow diet. Impaired glucose tolerance was observed following an intraperitoneal glucose bolus (Figure 3M), and no differences in insulin sensitivity were seen between genotypes (Figure 3N). The average size of inguinal and perigonadal adipocytes in female *Pdgfra*14-3-3 ζ KO mice were significantly increased by up to 2-fold (Figure 3O–Q). Whole-body fat mass was also significantly increased by 1.7-fold (Figure 3R), and perigonadal WAT mass increased by 3-fold (Figure 3T). No effects on lean mass were observed following 14-3-3 ζ deletion in APCs (Figure 3S). Levels of *Srebf1* and *Col1a1* mRNA were significantly decreased in both fat depots of *Pdgfra*14-3-3 ζ KO

female mice, and metabolic genes, such as *Hsl*, *Atgl*, and *Slc2a4* were significantly downregulated only in perigonadal fat (Sup. Fig. 3F), suggesting an impact on adipocyte metabolism in white adipose tissue. Altogether, results obtained male and female *Pdgfra14-3-3ζ*KO mice indicate that 14-3-3ζ exerts prominent effects on APCs to influence postnatal adiposity.

2.5. The impact of 14-3-3ζ deletion on adiposity in female *Pdgfra14-3-3ζ*KO mice is independent of food intake and metabolism

Since *Pdgfra*⁺ fibroblasts are present in a variety of tissues [26–28], we questioned if *Pdgfra*-Cre-mediated 14-3-3ζ deletion in female mice would impact other physiological axes that regulate feeding behavior and metabolic homeostasis (Figure 3K–T). When *Pdgfra14-3-3ζ*KO female mice were placed in metabolic cages, no differences in food intake were observed (Sup. Fig. 5A,B). Although female *Pdgfra14-3-3ζ*KO mice displayed decreased energy expenditure at various time-points, mostly during dark phases (Sup. Fig. 5C), overall energy expenditure was unaltered when compared to WT mice (Sup. Fig. 5D). This was consistent with our previous work where food intake and energy expenditure were unchanged after whole body knockout of 14-3-3ζ [9]. Similarly, fatty acid oxidation rates in *Pdgfra14-3-3ζ*KO female mice were not affected (Sup. Fig. 5E and F).

To further assess whether 14-3-3ζ acts in APCs, we isolated and cultured SVF from inguinal adipose tissues of male and female WT and *Pdgfra14-3-3ζ*KO mice, followed by inducing adipogenesis (Figure 3U). Deletion of 14-3-3ζ in *Pdgfra*⁺ APCs of female mice was found to only significantly enhance adipogenesis, based on Oil Red-O staining, a surrogate measure of lipid content (Figure 3V–Y). Additional, detailed molecular insights beyond ORO staining can also be used to determine if and how adipogenesis is governed by 14-3-3ζ within APCs and if this is a cell-autonomous phenomenon.

2.6. Deletion of 14-3-3ζ in APCs does not protect against HFD-induced obesity

As 14-3-3ζ appeared to exert its effects at the level of APCs, we further questioned the impact of HFD feeding on *Pdgfra14-3-3ζ*KO mice. When fed a HFD for 15 weeks, *Pdgfra14-3-3ζ*KO males, compared to WT, were not protected against body weight gain (Sup. Fig. 4A) or increases in total fat mass (Sup. Fig. 4B); Slight increases in inguinal and gonadal fat masses were observed, but this did not impact the average size of inguinal and perigonadal adipocytes (Sup. Fig. 4C–F). Glucose tolerance and insulin sensitivity were slightly improved in *Pdgfra14-3-3ζ*KO male mice (Sup. Fig. 4G,H), as well as liver weights (Sup. Fig. 4I). Unexpectedly, deletion of 14-3-3ζ in APCs did not influence body weight, adiposity, glucose homeostasis, or liver weights in female mice fed a HFD (Sup. Fig. 4J–R). Collectively, these observations demonstrate that embryonic deletion of 14-3-3ζ in APCs does not confer protection against HFD-induced obesity.

2.7. 14-3-3ζ is heterogeneously expressed by mature adipocytes and APCs

The limited impact on adiposity and body weight due to 14-3-3ζ deletion in APCs of chow and HFD-fed *Pdgfra14-3-3ζ*KO male mice was unexpected (Figure 3A–J). We anticipated that deletion in APCs would block adipogenesis similar to our previous findings in 3T3-L1 preadipocytes [9]. Hence, we hypothesized that 14-3-3ζ might be heterogeneously expressed in different APCs populations, as well as in certain mature adipocyte niches. Indeed, we previously observed

heterogenous expression of 14-3-3ζ in mature adipocytes in gonadal adipose tissues of male mice [10]. We took advantage of the publicly available mouse white adipose tissue atlas by Emont et al. [23] (Sup. Fig. 6), and re-analysis of the single-nuclei RNA-Seq dataset of mature adipocyte and APC clusters revealed that a small fraction of cells expresses *Ywhaz* (Sup. Fig. 6). An important caveat in this dataset is that it is not possible to distinguish cells not expressing *Ywhaz* from dropouts due to the inherent low reads per nuclei from single-nuclei sequencing. Mature adipocytes with detectable levels of *Ywhaz* mRNA represented nearly 15% and 30% of total mature adipocytes in males and females, respectively (Sup. Fig. 6A–E), and APCs with detectable levels of *Ywhaz* represented 17% and 19% of APCs in males and in females, respectively (Sup. Fig. 6F–J). The low proportion of *Ywhaz*-expressing mature adipocytes or APCs may partly explain the mild phenotypes of our *Adipoq14-3-3ζ*KO and *Pdgfra14-3-3ζ*KO mice, but despite this, we still aimed to further define the regulatory mechanisms underlying 14-3-3ζ-dependent adipogenesis.

2.8. Generation of TAP-tagged 14-3-3ζ expressing 3T3-L1 cells to interrogate the nuclear 14-3-3ζ interactome

14-3-3 proteins are not *bona fide* transcription factors as they do not contain DNA-binding domains [29]. With the ability of 14-3-3 proteins to interact with metabolic transcription factors, such as FOXO1 and the CREB coactivators CRTC1 and CRTC2 [30,31], it seemed plausible that 14-3-3ζ may influence the differentiation of preadipocytes by binding to and nucleating adipogenic transcriptional complexes. In fact, we previously showed that 14-3-3ζ interacts with C/EBP-β during adipogenesis [9]. As we previously reported that affinity proteomics can be used to elucidate the 14-3-3ζ interactome under physiological and pathophysiological contexts [11,12], we sought to define the nuclear 14-3-3ζ interactome during the differentiation of preadipocytes, with the goal of identifying novel adipogenic transcription factors or co-regulators anchored or regulated by 14-3-3ζ.

To this end, CRISPR-Cas9 editing was used to generate TAP (FLAG-hemagglutinine (HA))-tagged 14-3-3ζ-expressing 3T3-L1 preadipocytes, which were originally derived from a male mouse (TAP-3T3-L1, Sup. Fig. 7A–E). This strategy was chosen to avoid artifacts associated with protein overexpression, as the TAP-14-3-3ζ molecule is expressed at endogenous levels [32,33] (Sup. Fig. 7E,G). Using non-edited (WT) 3T3-L1 cells as a benchmark comparator for adipogenesis, we confirmed that CRISPR-Cas9-edited TAP-3T3-L1 cells maintained their adipogenic potential in response to MDI and MDIR, which makes them appropriate to use as a model to identify the nuclear 14-3-3ζ interactome during adipogenesis (Sup. Fig. 7F,H–M).

The adipogenic potential of TAP-3T3-L1 cells was indeed validated by Oil Red-O staining (Sup. Fig. 7H,I), triglyceride storage (Sup. Fig. 7J), isoproterenol-induced lipolysis (Sup. Fig. 7K,L), and mRNA expression and nuclear accumulation of PPARγ1/2 after induction with MDI and MDIR (Sup. Fig. 7F,M). We also confirmed that insertion of TAP-tag did not affect the expression of the remaining 14-3-3 isoforms (Sup. Fig. 7G). It is important to note that in the process of generating the TAP-3T3-L1 cell line, by the selection and propagation of a single cell clone, cells were passed for 16 passages. This relatively high passage number is known to reduce the adipogenic potential of 3T3-L1 cells and likely accounts for the lower differentiation efficiency in response to MDI as compared to WT 3T3-L1 cells. This could be circumvented with the addition rosiglitazone, a PPARγ agonist [34], to the differentiation cocktail (MDIR), which confirmed the ability of TAP-3T3-L1 cells to fully differentiate into adipocytes (Sup. Fig. 7F,H–M).

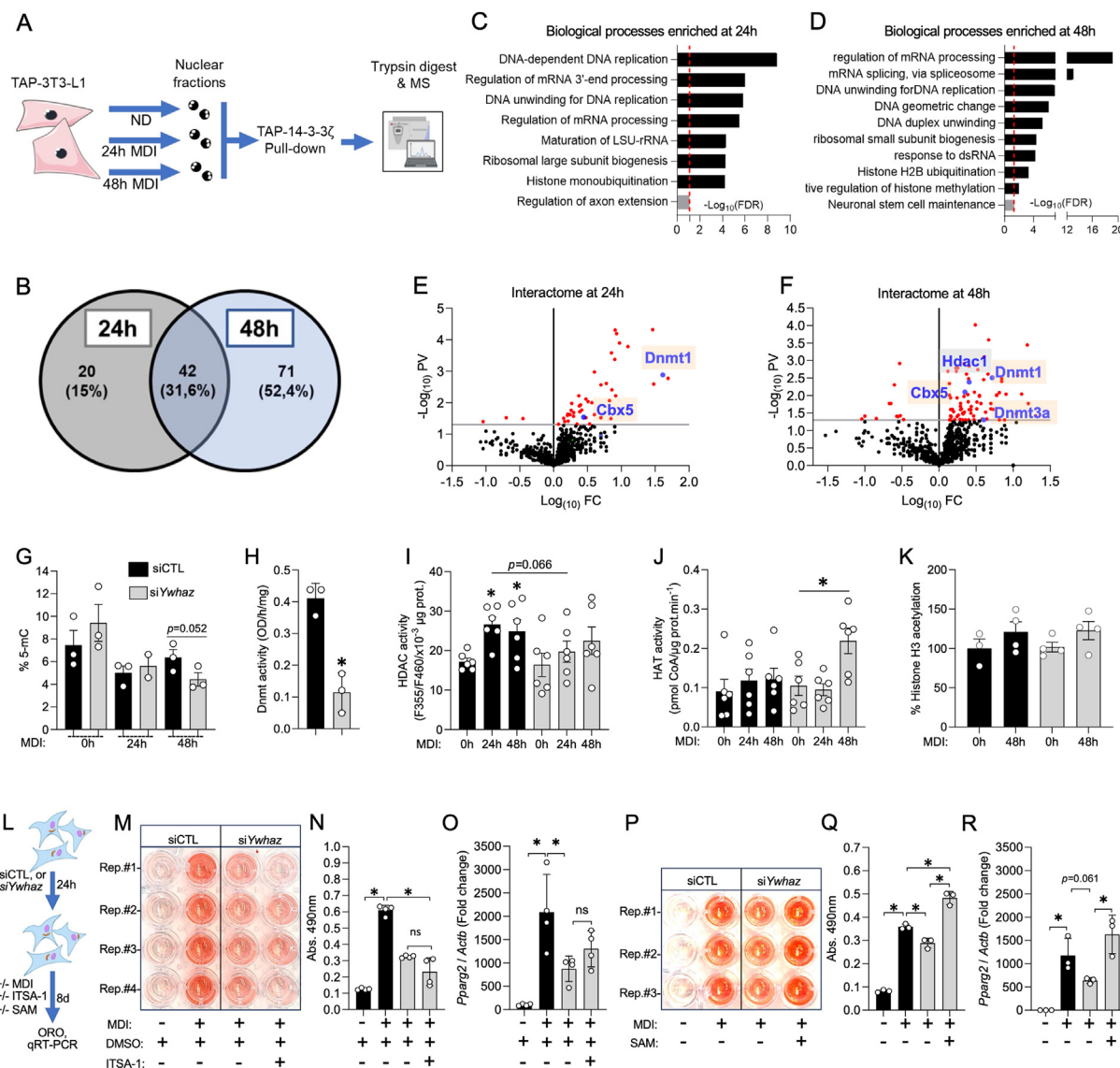


Figure 4: Key effectors of chromatin accessibility are influenced by 14-3-3 ζ as part of its nuclear interactome during the early step of adipogenesis. (A) Schematic outline of how TAP-3T3-L1 cells were used to elucidate the nuclear interactome of 14-3-3 ζ during the first 24 and 48 h of adipogenesis ($n = 4$ for each condition). (B) Venn diagram showing the number of unique and overlapping proteins enriched at 24 h and 48 h post induction. (C,D) GO analysis showing the most enriched Biological Processes attributed to 14-3-3 ζ interactome at 24 h (C) and 48 h (D) of adipogenesis. (E,F) Volcano plots of the decreased and enriched proteins in the 14-3-3 ζ nuclear interactome. (G–K) Genomic DNA (G), crude nuclear fractions (H), nuclear protein fractions (I,J), and Histone fractions (K) extracted from 3T3-L1 cells transfected for 48 h with siCTL (10 nM) or siYwhaz (10 nM) were respectively used for assessing whole 5-mC (G), DNMT activity (H), HDAC (I) and HAT (J) activity, and histone H3 acetylation level (K), normalized by total protein ($n = 3–6$ for each condition). (L) Schematic outline of how siCTL- or siYwhaz- (10 nM each) transfected 3T3-L1 cells were subjected to an 8-day MDI differentiation protocol in the presence or absence of either ITSA-1 or S-adenosylmethionine (SAM, 100 μ M each) prior to Oil Red-O staining and RNA extraction for qRT-PCR. (M–R) Oil Red-O staining (M,P), Oil Red-O quantification measured by absorbance at 490 nm (O, Q), and mRNA expression level of *Pparg2* (O, R) after co-treatment of differentiating 3T3-L1 with ITSA-1 (M–O) or SAM (P–R). Error bars represent S.E.M. Significant differences between conditions are indicated by * $P < 0.05$ (calculated by Student's t-test). Figure was partly generated with Biorender (A). (For interpretation of the references to color in this figure legend, the reader is referred to the Web version of this article.)

2.9. Nuclear 14-3-3 ζ interactors are associated with ribosomal biogenesis, RNA processing, DNA replication, and chromatin architecture during adipogenesis.

Affinity proteomics was performed on nuclear TAP-14-3-3 ζ complexes collected from TAP-3T3-L1 cells after 24 h and 48 h treatment with MDI (Figure 4A). These time points were chosen to identify proteins that associate with 14-3-3 ζ during the first 48 h of adipogenesis, the critical, early period when signaling events necessary for murine adipogenesis occur [4,5,9,11]. At 24 h and 48 h post-differentiation, mass spectrometry revealed that the 14-3-3 ζ nuclear interactome was significantly

enriched with 62 and 113 proteins, respectively ($FC \geq 1.5$, $p \leq 0.05$; Figure 4B; Sup. Tables 1 and 2). Contrary to our initial objective of discovering novel adipogenic transcription factors or regulators, the only transcription factor that we detected was C/EBP- β (Sup. Tables 1 and 2). To gain insights into the functional roles of identified proteins in the TAP-14-3-3 ζ interactome at both time points, gene ontology analysis was performed. Nuclear 14-3-3 ζ interacting proteins were primarily associated with histone H2B ubiquitination, DNA unwinding for replication, DNA hypermethylation and ribosome assembly ($FDR \leq 0.001$, $\text{Log}_{10}\text{Fold Enrichment} \geq 1.0$) (Figure 4C,D). We also observed proteins involved in

RNA splicing and maturation (Figure 4C,D), in line with our previous finding that 14-3-3 ζ interactome contains RNA-splicing factors playing essential roles in adipogenesis [11].

To gain an understanding of the abovementioned biological functions in adipogenesis, we assessed how interfering in these processes would affect adipocyte differentiation (Sup. Fig. 8A–D). As revealed by ORO staining, Etoposide, a classic inhibitor of DNA unwinding [35], as well as Acivicin and Streptonigrin, two inhibitors of ribosome biogenesis and assembly [36], significantly impeded 3T3-L1 differentiation when administered during the first 48 h or during the full process of differentiation (Sup. Fig. 8A,B). Exposure of 3T3-L1 cells to Tacedinaline and Ciprofloxacin, which are inhibitors of Histone deacetylation and minichromosome maintenance proteins (MCM2-7), respectively, potentiated adipogenesis (Sup. Fig. 8A,B). Of note was the observation that MCM proteins were found to be among the most highly enriched proteins in the nuclear 14-3-3 ζ interactome (Sup. Tables 1 and 2). We also used siRNAs to deplete various 14-3-3 ζ interactors with central roles in DNA unwinding and replication (MCM2-7) [37], histone modifications (CTR9, PAF1 and LEO1) [38,39], RNA processing (NOP2) [40] and ribosome assembly (PES1, RSL1D1 and LAS1) [41] (Sup. Fig. 8C,D). Depletion of these proteins mostly impaired adipogenesis as assessed by Oil Red-O staining (Sup. Fig. 8C) and *Pparg2* expression (Sup. Fig. 8D), except for depletion of LEO1 which significantly potentiated *Pparg2* expression. These findings support important regulatory roles of nuclear 14-3-3 ζ interactors on adipogenesis.

2.10. 14-3-3 ζ regulates the activity of DNMTs, HDACs and HATs

With significantly increased abundance of DNA methyltransferases 1 and 3a (DNMT1 and DNMT3A), Chromobox protein homolog 5 (CBX5), and Histone deacetylase 1 (HDAC1) within the 14-3-3 ζ nuclear interactome (Figure 4E, F), this suggested that 14-3-3 ζ might regulate the activities of these key epigenetic modifiers [42,43]. Silencing of *Ywhaz* in 3T3-L1 cells led to a 30% decrease in whole methylation of carbon-5 of cytosine (5-mC), a critical epigenetic mark targeted by DNMTs (Figure 4G). In a similar vein, silencing *Ywhaz* mRNA strikingly decreased by 4-fold the activity of DNMT enzymes [44] (Figure 4H). Total HDAC activity was significantly increased by up to 1.5-fold after 24 h and 48 h of differentiation in 3T3-L1 cells transfected with siCTL (Figure 4I); however, this increase was abrogated when cells were treated with si*Ywhaz* (Figure 4I). This suggests a functional interaction between 14-3-3 ζ and HDAC enzymes during the early stages of differentiation. Although we did not identify histone acetyltransferase (HAT) in the 14-3-3 ζ interactome, we explored its dependence on *Ywhaz* expression, since it is an important modulator of histone acetylation by acting as an antagonist to HDACs. Silencing of *Ywhaz* resulted in a significant increase of HAT activity by up to 2-fold at 48 h of differentiation, and this was not detected in differentiating cells normally expressing *Ywhaz* (Figure 4J). However, global acetylation of Histone-3, which is under the influence of HDACs and HATs [45], remained unchanged during differentiation and following *Ywhaz* silencing (Figure 4K).

Co-treatment of MDI-stimulated, *Ywhaz*-depleted 3T3-L1 cells with Inhibitor of Trichostatin 1 (ITSA-1), an HDAC activator [46,47], failed to restore their adipogenic potential, as shown by Oil Red-O staining and *Pparg2* mRNA levels (Figure 4L–O). However, when co-treated with S-Adenosyl-L-methionine (SAM), a methyl donor and primary substrate for DNMT-mediated DNA methylation (Figure 4L) [48], adipogenic differentiation of si*Ywhaz*-transfected cells exceeded that of control cells (Figure 4P–R).

Overall, silencing of *Ywhaz* at early timepoints of adipogenesis blocked HDACs activity, increased HAT activity, and reduced whole 5-

methylcytosine (5-mC, DNA methylation). In parallel, re-activation of DNMT activity using SAM rescued adipogenesis. Collectively, these observations support that 14-3-3 ζ , through direct or indirect interactions, balances the activity of key effectors of chromatin accessibility that are crucial to the initiation and progression of adipogenesis.

2.11. 14-3-3 ζ influences chromatin remodeling during adipogenesis

To explore if 14-3-3 ζ regulates chromatin accessibility during adipocyte differentiation, we performed ATAC-seq on siCTL- or si*Ywhaz*-transfected 3T3-L1 cells undergoing MDI-induced differentiation (Figure 5A). Compared to siCTL-transfected cells, 14-3-3 ζ depletion decreased accessibility of 215, 1,244 and 943 distinct chromatin regions at 0 h, 24 h and 48 h post-MDI induction, respectively (fold change ≤ 0.50 and *p. adj.* ≤ 0.05) (Figure 5B). Among these chromatin regions with decreased accessibility, 34 and 353 overlapped with either the three timepoints or the 24 h and 48 h timepoints (Figure 5B). Conversely, increased accessibility of 138, 1,756 and 821 chromatin regions (fold change ≥ 1.50 and *p. adj.* ≤ 0.05) was seen at the three timepoints, with 22 and 461 overlapping with the three timepoints and the 24 h and 48 h timepoints, respectively (Figure 5C).

Using the GREAT (v.4.0.4) and ShinyGO (v.0.82) [49,50], we associated these significantly, differentially accessible chromatin regions with genes and annotated these genes by Gene Ontology ($-\log_{10}FDR \geq 3$), respectively (Figure 5D–G). Genes associated with “development” and “regulation of cell differentiation” were among those whose accessibility were decreased at 24 h post MDI and after *Ywhaz* silencing (Figure 5D). After 48 h of differentiation, depletion of *Ywhaz* decreased the accessibility of genes associated with adipocyte processes, including adaptive thermogenesis, neutral lipid metabolic processes, and lipid metabolic processes (Figure 5F). Genes with increased accessibility at both time points in presence of si*Ywhaz* were not related to adipocyte function or development, but rather to fibroblast characteristics (Figure 5E,G). Following depletion of 14-3-3 ζ , coverage tracks of ATAC-seq signals showed significantly reduced accessibility of two genes involved in adipogenesis or adipocyte function, namely *Adig* (promoter region), which encodes Adipogenin [51], and *Fabp4* (exon 1), which encodes Fatty acid binding protein 4 [52] (Figure 5H,I). Motif enrichment analysis further revealed that when compared to control conditions, depletion of 14-3-3 ζ significantly ($-\log_{10}p \geq 5$) decreased the accessibility of 47 enhancers (overlapping with H3K27ac marks and lacking H3K4me3 marks, Sup. Table 3) and 16 promoters (overlapping with H3K4me3 marks, Sup. Table 4) 24 h post-MDI induction. After 48 h of MDI treatment, depletion of 14-3-3 ζ significantly ($-\log_{10}p \geq 5$) decreased the accessibility of 28 enhancers (Sup. Table 5) and 11 promoters (Sup. Table 6). Among the promoters and enhancers with significantly decreased accessibility at both differentiation timepoints, we identified elements crucial to adipogenesis, such as Peroxisome proliferator-activated receptor alpha (*PPARA*), Retinoic X receptor (*Rxr*) and Peroxisome proliferator-activated receptor elements (*PPARE*) (Figure 5J,K). Exhaustive lists of the downregulated enhancers and promoters at both time points are presented in Sup. Tables 3–6. Altogether, our ATAC-seq results indicate that depletion of 14-3-3 ζ during the early stages of adipogenesis impacts the accessibility of distinct chromatin regions at various pro-adipogenic genes.

2.12. 14-3-3 ζ enables both accessibility and expression of adipogenic genes at early stages of adipogenesis

To assess how changes in chromatin accessibility correlate with changes in gene expression in the context of 14-3-3 ζ -regulated

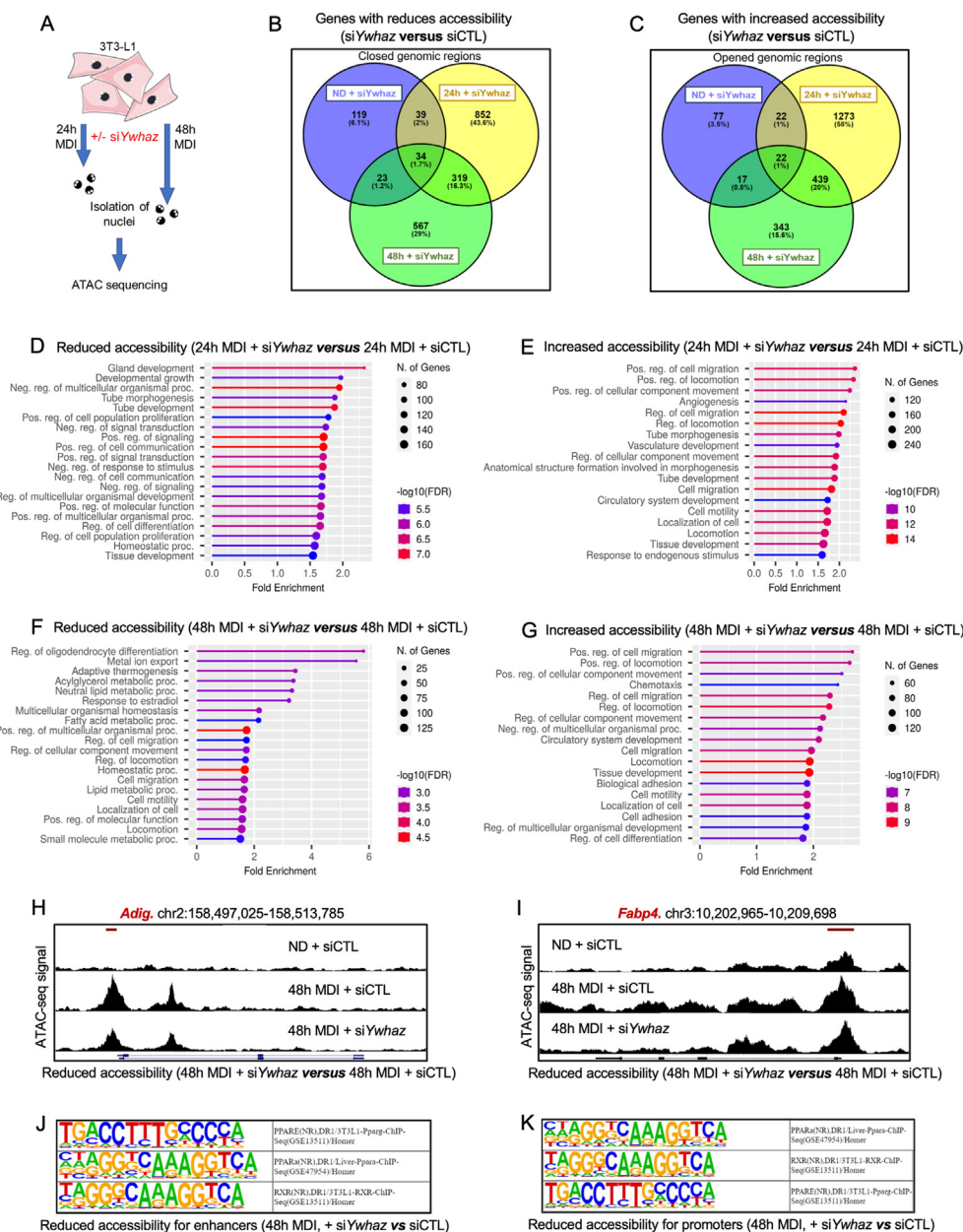


Figure 5: 14-3-3 ζ is involved in chromatin remodeling and accessibility during adipogenesis. (A) Schematic overview of the use of 3T3-L1 preadipocytes for ATAC-seq, 24 h and 48 h post-differentiation with MDI following transfection with siCTL or siYwhaz (10 nM each). (B,C) Venn diagrams showing overlap of (B) down-regulated or (C) up-regulated differentially accessible regions after siYwhaz treatment at 0, 24 and 48 h post-MDI induction. (D,E) Coverage tracks of ATAC-seq signals at the *Fabp4* (D) and *Adig* (E) genes. (F,G) Enhancers (F) and promoters (G) motif enrichment analysis at 48 h post-MDI induction in presence of siYwhaz. Figure was partly generated with Biorender (A).

adipogenesis, we integrated our ATAC-seq results with our previously published RNA-seq dataset (GSE60745, Figure 6A) derived from 3T3-L1 cells treated for 0 h, 24 h or 48 h with MDI in presence of either siCTL or siYwhaz [9]. These conditions correspond to what was used in our proteomic and ATAC-seq studies (Figures 4A and 5A). Our integrated analysis of ATAC-seq and RNA-seq did not reveal correlations between chromatin accessibility and changes in genes expression due to 14-3-3 ζ silencing at 24 h of differentiation (Figure 6B). However, following 48 h of differentiation, silencing of 14-3-3 ζ resulted in a positive and significant correlation ($r > 0.4$, $p \leq 0.05$) between differentially accessible promoters and differentially expressed genes (Figure 6C). Interestingly, *Fabp4* was found to be among the negatively

regulated genes for both promoter accessibility and RNA expression at 48 h of differentiation (Figure 6C). Moreover, *Retn* and *Fam83a*, which respectively encode Resistin and Family with sequence similarity 83 A (Fam83A) proteins, were also among the genes with decreased promoter accessibility and expression at the same timepoint (Figure 6C). Both *Retn* and *Fam83a* have previously been established as strictly required for adipogenesis [53,54]. Collectively, these findings confirmed that at early stages of adipogenesis, 14-3-3 ζ is a permissive factor that promotes a landscape of chromatin accessibility that enables the expression of adipogenic genes. To further confirm that 14-3-3 ζ regulates the accessibility of chromatin regions of pro-adipogenic genes, we explored if over-expression of key

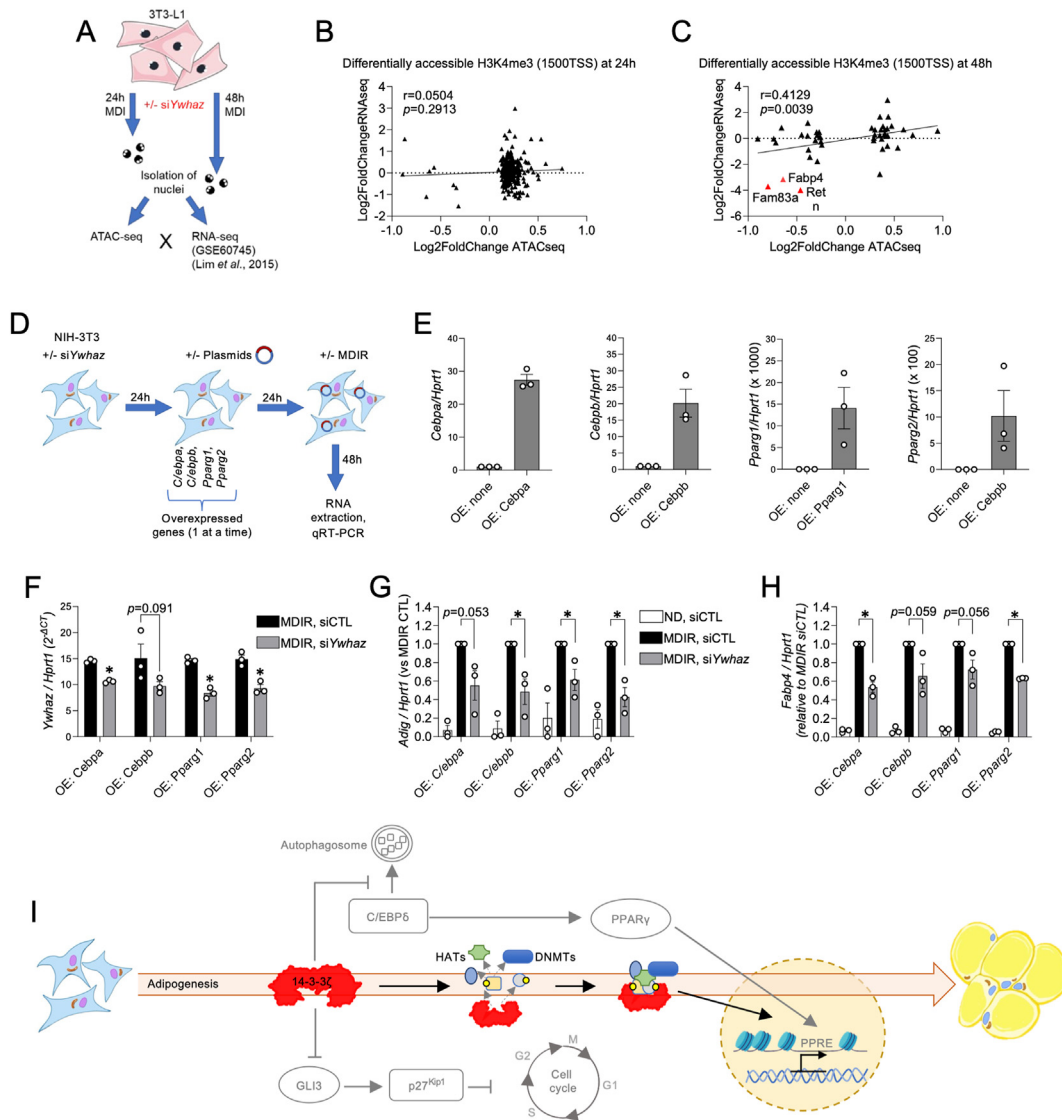


Figure 6: 14-3-3 ζ enables accessibility and the transcription of genes involved in adipocyte maturation and function. (A) Over-laying of ATAC-seq results with previous RNA-seq results (GSE60745) to correlate differentially accessible promoter regions with fold-changes in expression of corresponding genes, (B) 24 h and (C) 48 h post-MDI induction in presence of siYwhaz. (D) Experimental outline to assess requirement of 14-3-3 ζ for active ATF-dependent expression of adipogenic genes. (E) Quantification of *Cebpa*, *Cebpb*, *Pparg1*, and *Pparg2* mRNA levels in NIH-3T3 cells transfected or not with plasmids containing *Cebpa*, *Cebpb*, *Pparg1*, or *Pparg2*. (F) *Ywhaz*, (G) *Adig*, and (H) *Fabp4* mRNA expression levels in NIH-3T3 cells successively transfected with siYwhaz (60 nM) and plasmids for *Cebpa*, *Cebpb*, *Pparg1*, and *Pparg2* prior to treatment with MDI for 48h. (I) Graphical illustration of the new proposed mechanism (bright colors) on how 14-3-3 ζ regulates adipogenesis via chromatin remodeling in integration with previously found mechanisms (dim colors) [9]. Figure was partly generated with Biorender (A,I). (For interpretation of the references to color in this figure legend, the reader is referred to the Web version of this article.)

ATFs could rescue the effect of 14-3-3 ζ depletion. We hypothesized that excessive over-expression of an ATF would be unable to promote differentiation if essential chromatin regions remain inaccessible after 14-3-3 ζ depletion. To this end, we used NIH-3T3 fibroblasts that normally lack the ability to differentiate into adipocytes. However, when ectopic ATFs such as C/EBP- β , C/EBP- α , or PPAR γ 2 are over-expressed, they acquire the capacity to undergo MDI-induced, or/and PPAR γ agonism (MDIR)-dependent adipogenesis [55,56]. NIH-3T3 cells were sequentially transfected with or without siYwhaz and plasmids encoding either C/EBP α , C/EBP β , PPAR γ 1 or PPAR γ 2, followed by MDI to induce differentiation (Figure 6D). Overexpression of *Cebpa*, *Cebpb*, *Pparg1*, and *Pparg2* and knock down of *Ywhaz* were confirmed by qRT-PCR (Figure 6E,F). Up to 10-fold induction of *Adig* and *Fabp4*

expression was detected in MDIR-treated NIH-3T3 cells overexpressing each ATF (Figure 6G,H); however, when 14-3-3 ζ was depleted, expression levels of *Adig* and *Fabp4* mRNA in response to MDI were significantly blunted by up to 50% and 40%, respectively (Figure 6G,H). These findings are consistent with our *in vitro* data that demonstrate that 14-3-3 ζ is required for accessibility of key adipogenic factors (Figures 4–6). Thus, 14-3-3 ζ plays a critical role in ensuring the accessibility of key chromatin regions involved in adipogenesis.

3. DISCUSSION

Our previous discoveries on the role of 14-3-3 ζ in adipogenesis were based on systemic loss- and gain-of-function mouse models [9,11],

and we sought to define which cell type, mature adipocytes or APCs, were key in the regulation of 14-3-3 ζ -dependent adiposity. Although deletion of 14-3-3 ζ in either cell population affected glucose tolerance, effects on body weight gain and adiposity were primarily seen when 14-3-3 ζ was deleted in APCs. Using CRISPR-Cas9 genome editing, we developed a useful model to explore the nuclear 14-3-3 ζ interactome of APCs during adipogenesis, and this led to the discovery that 14-3-3 ζ primarily acts during the early stages of adipocyte differentiation and aids in the reorganization of chromatin to promote the accessibility of adipogenic gene, promoter, and enhancer regions. These findings, combined with our prior research, broaden our understanding of the importance of 14-3-3 ζ in adipocyte development, metabolism, and glucose and lipid homeostasis [9,10,12,57]. Furthermore, our study clearly demonstrates for the first time that 14-3-3 ζ , a ubiquitously expressed molecular scaffold protein, has critical upstream regulatory roles in adipogenesis.

We first confirmed significant positive correlations between adipose expression of *Ywhaz* and both basal and HF/HS-diet-induced adiposity in mice from the HMDP [19] (Figure 1A–F). *In vitro*, we also confirmed that expression of *Ywhaz* increases during adipogenesis and is indispensable to this process (Figure 1G–L). These observations align with prior measures in metabolically unhealthy human obesity, where expression of 14-3-3 ζ and other isoforms were elevated in adipose tissue [58]. For example, *YWHAZ* was found upregulated, among other upregulated genes in omental adipose tissue of obese, type 2 diabetic patients, as compared with healthy non-obese and non-diabetic, obese patients [58]. Moreover, a recent GWAS by Ang et al. identified *YWHAZ* and *YWHAZ* among 74 highly interconnected genes associated with obesity [59]. Lastly, elevated expression profiles of 14-3-3 protein-coding transcripts, including the Zeta isoform, have been confirmed in pancreatic islets from human subjects with type 2 diabetes by our and others' recent studies [21,60]. Whether elevated levels of 14-3-3 transcripts or *YWHAZ* variants are causal or associative to adipogenesis and the pathogenesis of obesity and type 2 diabetes remains unexplored, but these observations suggest that *YWHAZ* may be a reliable marker for unhealthy metabolic outcomes, such as adiposity, elevated BMI and type 2 diabetes.

Constitutive deletion of 14-3-3 ζ in mature adipocytes from chow-fed male and female mice was without impact on adiposity (Figure 2) and the expression of key metabolic genes in adipose tissue (Sup. Fig. 1). However, mild perturbations in glucose tolerance were detected, suggesting direct or indirect contributions of adipose 14-3-3 ζ to whole-body glucose uptake. Indeed, previous studies have revealed important contributions of 14-3-3 proteins to the coordination of Rab GTPase-activating protein-dependent pathways that mediate insulin- and exercise-dependent translocation of GLUT transporters for glucose uptake by adipocytes and myocytes [61,62].

Additional studies are required to better assess how adipocyte-specific 14-3-3 ζ contributes to whole-body glucose homeostasis and if it is involved in crosstalk with other metabolically active tissues. For example, both 14-3-3 ζ and 14-3-3 β have been found in the protein cargos of secreted large adipocyte-derived vesicles [63]. Thus, 14-3-3 ζ could participate as part of the bioactive adipocyte secretome that modulates glucose and lipid homeostasis, together with adiponectin, leptin, ANGPTL4, and other adipocyte-derived secreted vesicles cargos (extracellular vesicles, EVs) [64]. Further supporting the notion that 14-3-3 ζ delivered by EVs could play an important role in metabolism is the finding that 14-3-3 ζ was found within human umbilical cord mesenchymal stem cell-derived small EVs (hucMSC-sEVs) [65] and that delivery of 14-3-3 ζ by EVs to diabetic rats with renal dysfunction could improve glycemia, body weight and renal functions [65]. These

avenues will be interesting to further explore in terms of glucose tolerance and insulin sensitivity, given our observed differences between chow- and HFD-fed *Adipoq14-3-3 ζ KO* and *Pdgfra14-3-3 ζ KO* mice.

When using a tamoxifen-induced conditional deletion approach, we previously found that 14-3-3 ζ deletion in mature adipocytes of adult mice did not result in a notable metabolic phenotype, except impaired lipolysis [10]. In human mature adipocytes, 14-3-3 β , ϵ , γ and ζ were recently identified by Yang et al. as interacting proteins with lipid droplets [66]. Subsequent functional studies focused on the 14-3-3 β isoform and confirmed its requirement for lipolysis [66]. We also found that in adipose tissues, mRNA levels of *Tnfa*, a key inflammatory marker, were abrogated in female *Adipoq14-3-3 ζ KO* mice (Sup. Fig. 1F). This observation is of potential interest for future studies due to the established contribution of inflammation to adiposity- and obesity-related metabolic disorders [67,68]. Taken together, these findings indicate that in mature adipocytes, 14-3-3 isoforms are primarily involved in adipocyte functions, such as glucose uptake and lipolysis, rather than regulating expansion or proliferation.

In terms of adipose tissue architecture, deletion of 14-3-3 ζ in mature adipocytes had no impact, in contrast to whole-body 14-3-3 ζ KO mice that were strikingly lean from birth [9]. This strongly suggested that 14-3-3 ζ was more likely to influence APCs. In the present study, we report that constitutive deletion of 14-3-3 ζ in *Pdgfra*+ cells was more impactful on adipocyte size and body weight, but in a sex-specific manner. In male mice, deletion of 14-3-3 ζ in APCs resulted in reduced body weight and a trend towards lowered fat mass. In female *Pdgfra14-3-3 ζ KO* mice, fat mass, as well as inguinal and perigonadal adipocytes sizes, were surprisingly doubled and glucose tolerance markedly impaired, without impacts on insulin sensitivity, food intake, and metabolic rate. These results reveal that 14-3-3 ζ deletion may favor adipogenesis in *Pdgfra*+ APCs rather than in mature adipocytes, an observation further confirmed by female *Pdgfra14-3-3 ζ KO* SVF cells displaying enhanced Oil Red-O accumulation *in vitro* following differentiation (Figure 3 X and Y). Of note, these observations conflict with our prior discovery that siRNA-mediated depletion of 14-3-3 ζ inhibited adipogenesis in 3T3-L1 fibroblasts and that whole-body deletion of 14-3-3 ζ decreased adiposity [9]. These discrepancies may be explained by the different models used. For example, 3T3-L1 cells are primarily fibroblasts while APCs in SVF can be divided into distinct subpopulations [23]. Moreover, our previous study only focused on male mice [9], whereas our study explored both sexes and identified a sexual dimorphism with respect to weight gain and adiposity.

The sex-specific role of 14-3-3 ζ in APCs in white adipose tissue development was surprising and may rely on regulatory functions of 14-3-3 ζ on steroid hormone signaling. The link between 14-3-3 ζ and its related isoforms on estrogen signaling has been demonstrated by interactions between 14-3-3 ζ and its related isoforms and estrogen receptor alpha (ER α), which limits ER α transcriptional activity [69,70]. Furthermore, ER α -specific deletion in APCs has shown that E2 stimulates APC proliferation and promotes adipocyte hyperplasia and expansion of fat mass in female mice [71]. Altogether, these findings suggest a direct role of 14-3-3 ζ in ER α -regulated adiposity and may partly explain our observed phenotype in female mice. Further studies are required to investigate in detail the contribution of 14-3-3 ζ to sexual dimorphisms in adipogenesis.

The expression of *Pdgfra* is not limited to APCs and is common to fibroblasts residing in a broad variety of mesenchymal tissues [26–28,72]. Thus, the *Pdgfra* promoter is not exclusively specific to APCs, and there exists the possibility that the sexual dimorphic effects

on adipogenesis and body weight from deleting 14-3-3 ζ in *Pdgfra*+ cells may be mediated by other cell types, aside from APCs. Further studies should address this limitation by using an inducible Cre-Lox approach, such as the *Pdgfra-CreER^{T2}* [27], which would allow for a postnatal deletion of 14-3-3 ζ in APCs [26]. However, we did not observe altered food behavior, energy expenditure, or fatty acid oxidation rates in female *Pdgfra*14-3-3 ζ KO mice, which displayed the most pronounced effects on adipogenesis. Moreover, we were able to recapitulate *in vitro* a significantly higher adipogenic potential of SVF cells from female *Pdgfra*14-3-3 ζ KO mice. These observations strongly indicate that the effects of 14-3-3 ζ deletion may be mediated via APCs themselves.

One possible reason to explain the difference in magnitude or nature of effects between both the *Adipoq*14-3-3 ζ KO and *Pdgfra*14-3-3 ζ KO and the whole-body KO mice could be the heterogeneity of the adipocyte and APC populations. It is now established that heterogeneous populations of adipocytes inhabit fat depots, and these adipocytes originate from different APCs [14,73]. Even within a given adipocyte (*i.e.*, *Adipoq*+) or APC (*i.e.*, *Pdgfra*+) population, different niches exist with different cellular and physiological fates [14,73]. With our previous discovery of heterogeneous expression of 14-3-3 ζ among mature gonadal adipocytes [10] and the heterogeneous expression of *Ywhaz* among APCs (Sup. Fig. 6) [23], this opens new avenue of research to define 14-3-3 ζ + and 14-3-3 ζ -niches and how they contribute to adipocyte development and function.

We further sought to determine the mechanisms by which 14-3-3 ζ influences APCs differentiation through deciphering its interactome during the early stages of adipogenesis. Our previous studies have already demonstrated the promising value of mining the 14-3-3 ζ interactome to identify novel regulators of adipogenesis [11,12]. For example, we recently identified plakoglobin, the homolog of the adipogenic inhibitor β -catenin, among proteins enriched in the 14-3-3 ζ interactome in visceral adipose tissue of mice subjected to HFD [12]. To increase the likelihood of detecting novel adipogenic transcriptional regulators, we developed a novel cell model to elucidate the nuclear 14-3-3 ζ interactome (Figure 4), and surprisingly, the only transcription factor that could be detected was C/EBP- β (Sup. Tables 1 and 2), which confirmed our previous observation [11]. Instead, we found that the 14-3-3 ζ interactome was enriched with regulators of DNA unwinding and chromatin accessibility (Figure 4). These findings are consistent with previously reported regulatory functions of 14-3-3 proteins on ribosomal subunits [74] and chromatin modifying enzymes [75,76]. Using ATAC-seq, we confirmed the requirement of 14-3-3 ζ at early timepoints of adipocyte differentiation in the accessibility and expression of several genes, such as *Fabp4*, *Adig*, *Retn* and *Fam83a* (Figure 6). Importantly, all four genes are known regulators and effectors of adipogenesis.

Our findings pinpoint a new role of 14-3-3 ζ in the epigenetic control of adipogenesis (Figure 6). They support the likelihood that 14-3-3 ζ modulates the activity of key chromatin modifying enzymes, including HDAC1 and DNMT proteins that are found in its nuclear interactome. HDAC enzymes consist of 18 mammalian isoforms that promote the condensation of chromatin with discrepant effects on adipogenesis [77,78]. HDAC1 has been shown to inhibit adipogenesis through repressing the C/EBP α promoter [77], while other isoforms, such as HDAC4/5, promote adipogenesis [79]. The exact mechanisms that control the balance between these isoforms remains poorly defined. Although we did not identify HAT enzymes as part of 14-3-3 ζ interactome, they are also of interest as they play antagonistic roles to HDAC by promoting chromatin opening. Through targeting H3K9, H3H18 and H3K27 histones, HAT enzymes promote adipogenesis by

triggering C/EBP β and PPAR γ expression [78]. DNMT enzymes are determinant for lean *versus* obesity-associated adipogenesis [80], and in humans and various preclinical models, DNA hypomethylation of *PPARG*, *ADIPOQ* and *FABP4*, and loss of function of DNMT3A and DNMT1 were reported to provoke aberrant obesogenic growth and impaired metabolic fitness [81,82]. Herein, we showed that SAM, a universal methyl donor known to activate DNMTs, but not ITSA-1, an HDAC activator, rescued the defect in adipogenesis that stemmed from 14-3-3 ζ depletion, confirming the mechanistic role of 14-3-3 ζ in the regulation of key players of chromatin remodeling during the initiation of adipogenesis. 14-3-3 ζ could therefore be a core player in the epigenetic determination of adipose fate, which consists of a new promising avenue in adipose and obesity studies [68].

In conclusion, we identify a novel role for 14-3-3 ζ as a key regulator of APC differentiation. However, whether it exerts its influence through cell-autonomous mechanisms in specific APCs remains to be determined. Our findings establish for the first time 14-3-3 ζ as a crucial contributor to chromatin remodeling during adipogenesis to allow for the early expression of adipogenic genes. While additional studies are still required to define downstream effectors that mediate 14-3-3 ζ 's effects on chromatin remodeling, our proteomic analysis revealed that epigenetic factors, such as DNMTs and HDACs, are important in the actions of 14-3-3 ζ during APCs differentiation. Lastly, our study demonstrates the ability of utilizing the 14-3-3 ζ interactome to expand our knowledge of processes involved in adipocyte development and, by extension, the pathogenesis of obesity.

4. MATERIAL AND METHODS

4.1. Adipose tissue gene expression—Phenotypic correlations in the Hybrid Mouse Diversity Panel (HMDP)

One hundred inbred strains of male and female mice were maintained on a standard lab diet (6% kcal from fat, Ralston Purina Company) until eight weeks of age and subsequently placed on a high-fat/high-sucrose diet (32% kcal from fat and 25% kcal from sucrose) for eight weeks [19]. Animals were measured for total body fat mass and lean mass by magnetic resonance imaging (MRI) with Bruker Minispec and software from Eco Medical Systems, Houston, TX every two weeks. After 8 weeks of HF/HS diet, retro-orbital blood was collected under isoflurane anesthesia after 4 h of fasting. Plasma insulin, glucose, and triglycerides were determined as previously described [19,83]. The HOMA-IR was calculated using the equation $[(\text{Glucose}) \times (\text{Insulin})]/405$ [84]. Gene expression was measured from flash-frozen perigonadal adipose tissue samples with Affymetrix HT_MG430A. Gene expression—phenotype correlations (biweight midcorrelation) and their significance were calculated with the bicor function in the WGCNA package in R [85].

4.2. Animal husbandry and metabolic testing

*Pdgfra*Cre (C57BL/6-Tg(*Pdgfra-cre*)1Clc/J, strain #013148, Stock #005304, The Jackson Laboratory, Bar Harbor, ME, USA) and *Adipoq*Cre (B6.FVB-Tg(*Adipoq-cre*)1Evdr/J, strain #028020, stock #028020, The Jackson Laboratory, Bar Harbor, ME, USA) mice were bred with *Ywhaz*^{fllox/fllox} mice [10,21] on a C57BL/6J genetic background (*Ywhaz*^{tm1c(EUCOMM)HMgu}, Toronto Centre for Phenogenomics, Toronto, ON, Canada). All mice were maintained on a standard chow diet (Teklad diet no.TD2918) under 12:12-h light—dark cycles in an environmentally controlled setting (21 °C) with free access to food and water. Animals were kept on the chow diet for the duration of the study. All procedures were approved by the *Comité institutionnel de protection des animaux* (CIPA) du CRCHUM (CIPA protocol

#CM20043GLS) and performed in accordance with CIPA guidelines at the University of Montreal Hospital research center.

4.3. *In vivo* metabolic testing and tissue collection

*Adipoq*Cre:*Ywhaz*^{flox/flox} (*Adipoq*14-3-3 ζ KO) mice and *Pdgfra*Cre:*Ywhaz*^{flox/flox} (*Pdgfra*14-3-3 ζ KO) mice, and their respective non-floxed controls (*Adipoq*Cre:*Ywhaz*^{wt/wt} and *Pdgfra*Cre:*Ywhaz*^{wt/wt}), were fed a chow diet until 26 or 16 weeks of age, respectively, or fed a high-fat diet (60% kcal from fat, Research Diets, D12492, Brunswick, NJ) from 10 to 20 or 10–25 weeks of age, respectively. Animals were weighed weekly, and assessed during two last weeks for glucose tolerance, insulin sensitivity, and fat and lean masses. For glucose tolerance tests (IpGTT), mice were fasted for 6 h and challenged with D-glucose (2 g/kg b.w.) by intraperitoneal injection. For insulin tolerance tests (IpITT), mice were fasted for 4 h and challenged with Humulin R insulin (0.5 U/kg b.w.; Eli Lilly, Toronto, ON, Canada) by intraperitoneal injection. Blood glucose was measured from the tail vein with a Contour Next EZ glucose meter (Ascencia Diabetes Care, Basel, Switzerland). Body composition was scanned with EchoMRI-100 Body Composition Analyzer (version 2008.01.18, EchoMRI LLC) at the Rodent Cardiovascular Core Facility of the CRCHUM. Immediately after euthanasia of mice, perigonadal and inguinal white adipose tissues were collected, weighed, and either flash-frozen in liquid nitrogen for subsequent extraction of RNA or fixed in 4% paraformaldehyde for histological analysis.

4.4. Stromal vascular fraction (SVF) isolation and culture

Inguinal (subcutaneous) white adipose tissue (SAT) was harvested from euthanized 6–8 weeks-old *Pdgfra*14-3-3 ζ KO and WT male and female mice. SAT samples were immediately placed in sterile phosphate-buffered saline (PBS, pH 7.4) and stored on ice upon processing. Adipose samples were minced into ~1–2 mm pieces using sterile blades under aseptic conditions. Minced tissues were transferred to a digestion buffer containing (KRBH; bovine serum albumin, 1%; collagenase type II, 1 mg/mL) and incubated at 37 °C for 30–45 min with gentle agitation. Digestion was stopped by adding an equal volume of cold PBS. The suspension was filtered through a 100 μ m nylon mesh to remove undigested tissue fragments. The filtrate was centrifuged (200 \times g) for 20 min at 4 °C. The floating adipocytes were either discarded or frozen for subsequent RNA extraction, and the pellet containing the SVF was partly frozen for subsequent RNA extraction or retained for cell culture in DMEM supplemented with 10% FBS and 1% P/S onto flasks (passage 0). SVF at passages 2-to-4 were plated in 6-well plates at a cell density of 2.5×10^5 cells/well, then allowed to reach full confluence before initiating MDIR-mediated differentiation 24 h later.

4.5. Metabolic cages phenotyping

Female *Pdgfra*14-3-3 ζ KO and littermate controls at 9 weeks of age were placed in metabolic cages, as previously done [8]. In brief, mice were singly housed in CLAMS cages (Columbus Instruments, Columbus, OH) with *ad libitum* access to water and chow diet, and they were maintained on a 12-hour light/dark cycle on the following schedule: 24 h at 22 °C for acclimatization, 48 h at 22 °C for measurements that included food intake, respiratory exchange ratio, locomotor activity (beam breaks), and energy expenditure.

4.6. Histology and histomorphometry

Immediately after dissection, perigonadal and inguinal white adipose samples were fixed in 4% PFA for 7 days and stored in 70% ethanol before embedding in paraffin. Sections of 10 μ m thickness were

deparaffinized, rehydrated, and stained with hematoxylin and eosin. Images were taken at 20X (Nikon Eclipse Ti2, Nikon Instruments Inc, Melville, NY, USA) and the size distribution of adipocytes was quantified with ImageJ (Ver. 1.52u) or Visiormorph™ (2023.09 \times 64, Visiopharm, Denmark) following our established procedure [10,86].

4.7. CRISPR-Cas9 knock-in

For the expression of Flag-HA-*Ywhaz* in 3T3-L1 cells, the method of CRISPR/CAS9 Knock-in was used, Guide RNAs (gRNAs) were designed using the “optimized CRISPR design” tool (<https://www.benchling.com/crispr>). Oligonucleotides with Bsb1 cleavage overhang were ordered from Life Technologies, annealed, and cloned into Cas9/GFP expressing vector (pX458 from Addgene #48138). The sequence (CATAACTGGATATTCTGTAA) near Start codon ATG were used as gRNA. For the YWHAZ donor template, left homology arms (495bp containing ATG star codon of *Ywhaz* gene) + Flag-HA + right homology arm (671bp) cassette was synthesized (Bio Basic, Toronto), then cloned into pGEN-HDR-RFP plasmid (dTomato expression plasmid).

The gRNA plasmid (1 μ g) and donor template plasmid (3 μ g) were introduced into 3T3-L1 cells (1×10^6 cell) by electroporation (LONZA, Basel, Switzerland). After 48 h of electroporation, GFP and RFP positive cells were sorted into 96 well plates for genotyping and cell culture. Genomic DNA was extracted with QuickExtract (Mandel Scientific, Laval) and PCR was performed with Flag F (caaggcagcagatgacaaaagtc) + 3’OUTR (CAGAGCCAACAACGTGAGGT) primers using Q5® High-Fidelity DNA Polymerase (New England Biolabs, MA, USA) according to the manufacturer’s protocol. For Wild type cells, there was no band and Knock in PCR product (992bp) were identified using agarose gel electrophoresis (Sup. Fig. 7D). Genomic DNA was extracted with QuickExtract (Lucigen) and PCR was performed ATG F (TGGAACTTCTGAACAGGTGGA) + 3’OUTR (CAGAGCCAACAACGTGAGGT) primers using Q5® High-Fidelity DNA Polymerase according to the manufacturer’s protocol. The PCR products were cloned into pMiniT vector. 12 independent recombinant plasmids were selected for Sanger DNA sequencing, with T7 and SP6 used as sequence primers. Following the initial transfection of sgRNAs and Cas9 plasmids, selection and propagation of a single cell clone, and sub-passaging to increase cell numbers, 3T3-L1 cells were passed for 16 passages.

4.8. Cell culture, transient transfections and treatments

3T3-L1 (10–20 passages), TAP-3T3-L1 (18–22 passages) and NIH-3T3 (10–20 passages) cells were used for experiments. Cells were maintained in DMEM medium supplemented with 10% newborn calf serum (NBCS) and 1% penicillin-streptomycin. Prior to differentiation, cells were seeded onto 12-well plates or dishes and maintained until confluence. Differentiation was induced following the well-established methods of MDI (DMEM supplemented with 10% FBS, 1% P/S, 500 μ M IBMX, 500 nM dexamethasone, and 172 nM insulin) or MDIR (DMEM supplemented with 10% FBS, 1% P/S, 500 μ M IBMX, 500 nM dexamethasone, and 172 nM insulin, 10 μ M rosiglitazone) [9,10,87]. Following MDI or MDIR treatments for 48 h, the medium was replaced with DMEM supplemented with 10% FBS and 172 nM insulin every 2 days. Differentiation was assessed by Oil Red-O staining, as we previously performed, or by measuring expression of key adipogenic genes, 48 h after MDI or MDIR treatments, by qRT-PCR. Knockdown of 14-3-3 ζ was performed by transfecting cells with siRNA against *Ywhaz* (*siYwhaz*, 25 μ M per well, s76189, Silencer Select siRNA, Ambion) or an equivalent concentration of a scrambled control siRNA (#4390844, Silencer Select Negative Control #1, Ambion) using Lipofectamine RNAimax (ThermoFisher Scientific), 24 h before

differentiation. Overexpression of either *Cebpa*, *Cebpb*, *Pparg1* or *Pparg2* in NIH-3T3 cells was performed by transfecting pcDNA3.1(–) rat C/EBP alpha (#12550, Addgene, Watertown, MA, USA), pcDNA-mC/EBPb (#49198, Addgene, Watertown, MA, USA), pSV Sport PPAR gamma 1 (#8886, Addgene, Watertown, MA, USA), or pcDNA3.1-PPARgamma2 (#78768, Addgene, Watertown, MA, USA) plasmids using Lipofectamine 3000 (ThermoFisher Scientific), following manufacturer instructions, 24 h before transfection of *siYwhaz* and 48 h before MDIR treatment.

4.9. RNA isolation and qPCR

Total RNA was isolated from 3T3-L1 and NIH-3T3 cells after differentiation and/or transfection or from 10 mg of mice visceral (perigonadal) adipose tissue (VAT), subcutaneous (inguinal) adipose tissue (SAT), or intrascapular brown adipose tissue (BAT), with Trizol (ThermoFisher Scientific). Afterwards, cDNAs were synthesized with the High-Capacity cDNA Reverse Transcription Kit (ThermoFisher Scientific) prior to qPCR-based measurement of mRNA with SYBR green chemistry on a Quant-Studio 6-flex real-time PCR system (ThermoFisher Scientific). All data were normalized to *Hprt1* or *Actb* by the 2-delta Ct method. All primers sequences are listed in [supplementary Table 7](#).

4.10. Immunoblotting

TAP-3T3-L1 and 3T3-L1 cells after 0, 24 and 48 h of MDI and MDIR treatment were lysed, followed by a cell fractionation protocol [88]. Cytosolic and nuclear protein fractions, supplemented with protease and phosphatase inhibitors, as well as benzonase for the nuclear fraction, (1:50 v:v), were prepared and resolved by SDS-PAGE, transferred to PVDF membranes, and immunoblotted with antibodies against PPAR γ 1/2, Lamin a/b, and GAPDH. Primary and HRP-linked secondary antibodies were used, and their respective dilutions into blocking solution (I-Block, ThermoFisher Scientific) are listed in [supplementary Table 8](#).

4.11. Proteomics (nuclear proteins precipitation, mass spectrometry and data analysis)

Nuclear extracts were obtained from TAP-3T3-L1 cells (\pm MDI treatment after 24 or 48h) using extraction buffer which contained 150 mM NaCl, 50 mM Hepes (pH 7.4), 1M Hexylene glycol, 0.5% Sodium deoxycholate, 0.1% SDS, 2 mM EGTA, 1 mM Na₃VO₄, and 1 mM Na₄F. A total amount of 1.5 mg of protein in a 1 mL volume was used for all pull-downs. For each sample, 50 μ L of anti-HA magnetic beads (#88836, Pierce) were added, followed by overnight rotation at 4 $^{\circ}$ C. On the subsequent day, samples underwent three washes with the extraction buffer and three additional washes with 50 mM NH₄HCO₃. Beads were then resuspended in 100 μ L of 50 mM NH₄HCO₃, to which 1 μ g of trypsin was added, followed by overnight incubation at 37 $^{\circ}$ C. An additional 1 μ g of trypsin was added the next day, and the incubation continued for 4 h at 37 $^{\circ}$ C. After centrifugation, the supernatants containing peptides were collected in a separate tube. The beads were then rinsed twice with 100 μ L of water, which was added to the collected peptides. Finally, formic acid was added to achieve a final concentration of 4%, and the samples were subjected to speed vacuum concentration prior to analysis by mass spectrometry.

Samples were reconstituted in formic acid 0.2% and loaded and separated on a homemade reversed-phase column (150 μ m i.d. x 150 mm) with a 56-min gradient from 0% to 40% acetonitrile (0.2% FA) and a 600 nl/min flow rate on an Easy-nLC II (Thermo Fisher Scientific), connected to an Orbitrap Fusion Tribrid mass spectrometer (Thermo Fisher Scientific). Each full MS spectrum acquired with a

60,000 resolution was followed by 20 MS/MS spectra, where the 12 most abundant multiply charged ions were selected for MS/MS sequencing. Raw files were searched with MaxQuant software version 1.3.0.3 and searched against the Uniprot Human database (<http://www.uniprot.org/>) release 2016_02 (17-Feb-2016) including the reversed database with 74,508 entries. General false discovery rate (FDR) for peptides was at 1.0% with decoy removal. Searches were performed at a 25-ppm precursor ion tolerance and 1.0 Da fragment ion tolerance, assuming full tryptic digestion with up to three missed cleavages. Correct peptide identifications were distinguished from incorrect using the target-decoy approach, coupled with linear discriminant analysis as described previously. Once peptides were filtered to an initial FDR of 1%, peptides were assembled into proteins and further filtered to a final protein-level FDR of 1%. All proteins of the same family were grouped, and isoforms of the same protein were considered as one. To estimate the abundance of proteins within eluates, we rely on total spectral counts. Peptides showing significant ($P < 0.05$, non-paired t-test) increase in counts at 24 h and 48 h post differentiation were considered as enriched in 14-3-3 ζ interactome at these timepoints. Corresponding protein lists were analyzed with Gene Ontology (ShinyGO, version 0.741) to categorize them on their biological functions.

4.12. Measurements of DNMT, HDAC, or HAT activity, and 5-mC and histone H3 acetylation

Crude nuclear protein fractions, histone fractions, or genomic DNA were isolated from 3T3-L1 cells, plated on 100 mm diameter dishes, treated with scrambled siRNA or si14-3-3 ζ , at 0, 24 and 48 h of MDI-induced differentiation following instructions of the manufacturer. Equal quantities of proteins were subjected to a DNA methyltransferase (DNMT) colorimetric activity assay (#ab113467Abcam, Toronto, ON, Canada), Histone deacetylase (HDAC) fluorometric activity assay (#ab156064, Abcam Toronto, ON, Canada), Histone acetyltransferase (HAT) colorimetric activity assay (#ab65352, Abcam Toronto, ON, Canada), and Histone H3 Acetylation colorimetric Assay Kit (#ab115102, Abcam Toronto, ON, Canada). DNA extracts were subjected to global 5-methyl cytosine colorimetric assay kit (#ab233486, Abcam Toronto, ON, Canada).

4.13. ATAC-seq and RNA-seq generation and analysis

Assay for Transposase-Accessible Chromatin using high-throughput sequencing (ATAC-seq) was performed following protocols adapted from Buenrostro et al. [89] and Batie et al. [90]. Following treatments, 3T3-L1 cells were washed on plates with PBS and exposed to cell lysis buffer (10 mM Tris-HCl, pH 7.4, 10 mM NaCl, 3 mM MgCl₂, 0.1% IGEPAL CA-630). After 10 min of incubation on ice nuclei were detached, centrifuged (600g, 10 min, 4 $^{\circ}$ C), and washed twice in PBS with repeated centrifugation. Pellets (nuclei fractions) were resuspended in transposition buffer (50% v/v 2X Tagment DNA (TD) Buffer (Illumina, 336 Cambridge, UK), 32% v/v PBS, 0.1% v/v Tween-20, 0.1 mg/mL Digitonin (Promega, Southampton, UK), supplemented with 5% v/v TDE1 Tagment DNA Enzyme (Illumina, Cambridge, UK) in nuclease free water (Sigma, Gillingham, UK), by gentle pipetting. The transposition reaction was initiated by incubation at 37 $^{\circ}$ C and stopped by cooling to 4 $^{\circ}$ C. Following DNA extraction, tagmented DNA was amplified by PCR in a reaction mix (5 μ L DNA, 2.5 μ L of 25 μ M forward primer (Nextera/Illumina i5 adaptors (Illumina)), 2.5 μ L of 25 μ M reverse primer (Nextera/Illumina i7 adaptors (Illumina)), 10 μ L of SYBR green reagent) with the following thermocycler program: 5 min 72 $^{\circ}$ C, 30 sec 98 $^{\circ}$ C and 11 cycles of 10 sec 98 $^{\circ}$ C, 30 sec 63 $^{\circ}$ C and 1 min 72 $^{\circ}$ C.

Adaptors were trimmed from the ATAC-seq reads using Trim Galore (<https://github.com/FelixKrueger/TrimGalore>) and reads aligned to mm10 with Bowtie2 [91]. Picard (<http://broadinstitute.github.io/picard/>) was used to assess library size distribution. Bowtie2 was also used for the alignment of 3T3-L1 adipocytes ChIP-seq reads: GSM535755 (H3K4me3) GSM535758 (H3K27ac) and GSM535740 (input) downloaded from series GSE21365 [92]. MACS2 [93] was used for peak calling. Quantification of peaks-associated ATAC-seq reads was performed using FeatureCounts [94]. RNA-seq data from GSE60745 [9] was realigned and quantified using Salmon [95]. Differential analysis of quantified peaks (ATAC-seq) and gene expression (RNA-seq) was performed with DESeq2 [96]. Bedtools [97] was used to integrate ATAC-seq and ChIP-seq. Transcript factor motif analysis and gene annotation of peaks for integration with gene expression data was performed with the annotatePeaks function of HOMER. Correlation analysis was performed in GraphPad prism with all annotated peaks or with a subset of peaks annotated within 1500 nucleotides of the closest transcription start site (TSS). Differentially open and closed regions were submitted to ShinyGO v0.741 for KEGG pathway enrichment analysis.

4.14. Single nuclei RNA-seq analysis to determine *Ywhaz* heterogeneity in APCs

Filtered datasets including metadata consisting of mature adipocytes or APC populations from 20-week-old mice of both sexes were obtained from Emont et al. [23], and further sub-setted to contain only chow fed animals. Samples raw counts were then extracted and normalized using SCTransform method [98] and integrated with Seurat v5. Data were visualized using Uniform Manifold Approximation and Projection (UMAP) and the normalized and log-transformed expression values were used for downstream visualizations.

Data availability

Proteomics data was deposited in ProteomeXchange through partner MassIVE as a complete submission and assigned MSV000094119 and PXD049695. It can be downloaded from <ftp://MSV000094119@massive.ucsd.edu>, using the password: Rial.

Assay for Transposase-Accessible Chromatin using high-throughput sequencing (ATAC-seq) data were deposited to the Gene Expression Omnibus.

Statistical analysis

All data are expressed as the mean \pm SEM. Data were analyzed by ANOVA followed by Dunnett or Bonferroni t-tests, or by Student's t-tests, and significance was achieved when $P \leq 0.05$. A minimum of $n = 3$ independent experiments were performed for analysis.

ACKNOWLEDGEMENTS

This work was supported by CIHR Project (PJT-153144) and NSERC Discovery (RPGIN-2017-05209) to GEL, as well as funding from the Cardiometabolic Health Diabetes, and Obesity (CMDO) Research Network (Jean-Davignon Young Investigator Award) and the Banting Research Foundation (Discovery Award). Infrastructure support was provided through a Canada Foundation for Innovation (CFI)- John Evans Leaders Fund (JELF-37405) to GEL. GEL holds the Canada Research Chair in Adipocyte Development. SAR was previously supported by a post-doctoral award from the Fonds de Recherche du Québec Nature et technologies (FRQNT). AV was supported by a Mitacs Accelerate Post-doctoral Award and by the Banting Research Foundation. The authors acknowledge Drs. Roger Cox and Samantha Laber (MRC Harwell

Institute, University of Oxford, UK) for discussions with ATAC-seq and sharing an optimized experimental protocol. The authors also acknowledge Dr Nhung Vuong-Robillard (CRCHUM) who developed and optimized the macros for morphological analysis of adipose tissue histosections with Visiomorph™. MC was supported by NIH grant R01DK118287 as well as American Diabetes Association Innovative Basic Science Award (1-19-IBS-105). PPR is supported by a CIHR Project grant (PJT-178154). AM-S was supported by a New Investigator Research Grant (MR/P023223/1) and a Project Grant (MR/X009912/1) by the Medical Research Council (MRC, UK). Proteomic analyses were performed by the Center for Advanced Proteomics Analyses (CAPA), a Node of the Canadian Genomic Innovation Network that is supported by the Canadian Government through Genome Canada. Figures 4, 6, and 7 were partly generated with Biorender and Servier Medical Art.

CRediT AUTHORSHIP CONTRIBUTION STATEMENT

S.A. Rial: Writing — review & editing, Writing — original draft, Visualization, Validation, Methodology, Investigation, Formal analysis, Data curation, Conceptualization. **Z. You:** Methodology, Investigation, Formal analysis. **A. Vivoli:** Investigation, Formal analysis, Data curation. **F. Paré:** Investigation, Data curation. **D. Sean:** Investigation, Formal analysis. **A. Alkhoury:** Investigation, Data curation. **G. Lavoie:** Investigation, Data curation. **M. Civelek:** Writing — review & editing, Writing — original draft, Investigation, Formal analysis, Data curation. **A. Martinez-Sanchez:** Writing — review & editing, Writing — original draft, Investigation, Formal analysis, Data curation. **P.P. Roux:** Writing — review & editing, Writing — original draft, Investigation, Formal analysis. **T.M. Durcan:** Methodology, Investigation, Writing - original draft, Writing - review & editing. **G.E. Lim:** Writing — review & editing, Writing — original draft, Validation, Supervision, Project administration, Methodology, Investigation, Funding acquisition, Formal analysis, Data curation, Conceptualization.

DECLARATION OF COMPETING INTEREST

The authors declare that they have no known competing financial interests or personal relationships that could have appeared to influence the work reported in this paper.

DATA AVAILABILITY

No data was used for the research described in the article.

APPENDIX A. SUPPLEMENTARY DATA

Supplementary data to this article can be found online at <https://doi.org/10.1016/j.molmet.2025.102159>.

REFERENCES

- [1] Choe SS, Huh JY, Hwang IJ, Kim JI, Kim JB. Adipose tissue remodeling: its role in energy metabolism and metabolic disorders. *Front Endocrinol* 2016;7:30.
- [2] Cristancho AG, Lazar MA. Forming functional fat: a growing understanding of adipocyte differentiation. *Nat Rev Mol Cell Biol* 2011;12(11):722–34.
- [3] Ying T, Simmons RA. The role of adipocyte precursors in development and obesity. *Front Endocrinol* 2020;11:613606.
- [4] Siersbaek R, Madsen JGS, Javierre BM, Nielsen R, Bagge EK, Cairns J, et al. Dynamic rewiring of promoter-anchored chromatin loops during adipocyte differentiation. *Mol Cell* 2017;66(3):420–435 e425.

- [5] Siersbaek R, Nielsen R, Mandrup S. Transcriptional networks and chromatin remodeling controlling adipogenesis. *Trends Endocrinol Metabol* 2012;23(2):56–64.
- [6] Diallo K, Oppong AK, Lim GE. Can 14-3-3 proteins serve as therapeutic targets for the treatment of metabolic diseases? *Pharmacol Res* 2019;139:199–206.
- [7] Rial SA, Shishani R, Cummings BP, Lim GE. Is 14-3-3 the combination to unlock new pathways to improve metabolic homeostasis and β -Cell function? *Diabetes* 2023;72(8):1045–54.
- [8] Diallo K, Dussault S, Noll C, Lopez AF, Rivard A, Carpentier AC, et al. 14-3-3 ζ mediates an alternative, non-thermogenic mechanism in male mice to reduce heat loss and improve cold tolerance. *Mol Metabol* 2020;41:101052.
- [9] Lim GE, Albrecht T, Piske M, Sarai K, Lee JTC, Ramshaw HS, et al. 14-3-3zeta coordinates adipogenesis of visceral fat. *Nat Commun* 2015;6:7671.
- [10] Oppong AK, Diallo K, Robillard Frayne I, Des Rosiers C, Lim GE. Reducing 14-3-3 ζ expression influences adipocyte maturity and impairs function. *Am J Physiol Endocrinol Metab* 2020;319(1):E117–32.
- [11] Mugabo Y, Sadeghi M, Fang NN, Mayor T, Lim GE. Elucidation of the 14-3-3 ζ interactome reveals critical roles of RNA-splicing factors during adipogenesis. *J Biol Chem* 2018;293(18):6736–50.
- [12] Abou Azar F, Mugabo Y, Yuen S, Del Veliz S, Paré F, Rial SA, et al. Plakoglobin regulates adipocyte differentiation independently of the Wnt/ β -catenin signaling pathway. *Biochim Biophys Acta Mol Cell Res* 2024;119690.
- [13] Bäckdahl J, Franzén L, Massier L, Li Q, Jalkanen J, Gao H, et al. Spatial mapping reveals human adipocyte subpopulations with distinct sensitivities to insulin. *Cell Metab* 2021;33(9):1869–1882.e1866.
- [14] Marcelin G, Ferreira A, Liu Y, Atlan M, Aron-Wisniewsky J, Pelloux V, et al. A PDGFR α -Mediated switch toward CD9(high) adipocyte progenitors controls obesity-induced adipose tissue fibrosis. *Cell Metab* 2017;25(3):673–85.
- [15] Rodeheffer MS, Birsoy K, Friedman JM. Identification of white adipocyte progenitor cells *in vivo*. *Cell* 2008;135(2):240–9.
- [16] Cho DS, Lee B, Doles JD. Refining the adipose progenitor cell landscape in healthy and obese visceral adipose tissue using single-cell gene expression profiling. *Life Sci Alliance* 2019;2(6).
- [17] Sun C, Sakashita H, Kim J, Tang Z, Upchurch GM, Yao L, et al. Mosaic mutant analysis identifies PDGFR α /PDGFR β as negative regulators of adipogenesis. *Cell Stem Cell* 2020;26(5):707–721.e705.
- [18] Corvera S. Cellular heterogeneity in adipose tissues. *Annu Rev Physiol* 2021;83:257–78.
- [19] Parks BW, Nam E, Org E, Kostem E, Norheim F, Hui ST, et al. Genetic control of obesity and gut microbiota composition in response to high-fat, high-sucrose diet in mice. *Cell Metab* 2013;17(1):141–52.
- [20] Wong AM, Patel TP, Altman EK, Tugarinov N, Trivellin G, Yanovski JA. Characterization of the adiponectin promoter + Cre recombinase insertion in the Tg(Adipoq-cre)1Evd mouse by targeted locus amplification and droplet digital PCR. *Adipocyte* 2021;10(1):21–7.
- [21] Mugabo Y, Zhao C, Tan JJ, Ghosh A, Campbell SA, Fadzeyeva E, et al. 14-3-3 ζ constrains insulin secretion by regulating mitochondrial function in pancreatic β -cells. *JCI Insight* 2022;7(8):e156378.
- [22] Joshi PA, Waterhouse PD, Kasaian K, Fang H, Gulyaeva O, Sul HS, et al. PDGFR α + stromal adipocyte progenitors transition into epithelial cells during lobulo-alveologenesis in the murine mammary gland. *Nat Commun* 2019;10(1):1760.
- [23] Emont MP, Jacobs C, Essene AL, Pant D, Tenen D, Colletuori G, et al. A single-cell atlas of human and mouse white adipose tissue. *Nature* 2022;603(7903):926–33.
- [24] Berry R, Rodeheffer MS. Characterization of the adipocyte cellular lineage *in vivo*. *Nat Cell Biol* 2013;15(3):302–8.
- [25] Wang QA, Song A, Chen W, Schwalie PC, Zhang F, Vishvanath L, et al. Reversible De-differentiation of mature white adipocytes into preadipocyte-like precursors during lactation. *Cell Metab* 2018;28(2):282–288.e283.
- [26] Rendon CJ, Sempere L, Lauver A, Watts SW, Contreras GA. Anatomical location, sex, and age modulate adipocyte progenitor populations in perivascular adipose tissues. *Front Physiol* 2024;15:141218.
- [27] Chung MI, Bujnis M, Barkauskas CE, Kobayashi Y, Hogan BLM. Niche-mediated BMP/SMAD signaling regulates lung alveolar stem cell proliferation and differentiation. *Development* 2018;145(9).
- [28] Chu-Tan JA, Rutar M, Saxena K, Aggio-Bruce R, Essex RW, Valter K, et al. MicroRNA-124 dysregulation is associated with retinal inflammation and photoreceptor death in the degenerating retina. *Investig Ophthalmol Vis Sci* 2018;59(10):4094–105.
- [29] Rittinger K, Budman J, Xu J, Volinia S, Cantley LC, Smerdon SJ, et al. Structural analysis of 14-3-3 phosphopeptide complexes identifies a dual role for the nuclear export signal of 14-3-3 in ligand binding. *Mol Cell* 1999;4(2):153–66.
- [30] Kenanov DN, Visser EJ, Virta JM, Sijbesma E, Centorri F, Vickery HR, et al. A systematic approach to the discovery of protein-protein interaction stabilizers. *ACS Cent Sci* 2023;9(5):937–46.
- [31] Chen H, Zhang H, Chen P, Xiang S. Structural insights into the interaction between CRTCs and 14-3-3. *J Mol Biol* 2021;433(7):166874.
- [32] Kintaka R, Makanae K, Moriya H. Cellular growth defects triggered by an overload of protein localization processes. *Sci Rep* 2016;6(1):31774.
- [33] Li Y. Commonly used tag combinations for tandem affinity purification 2010;55(2):73–83.
- [34] Day C, Bailey CJ. Rosiglitazone. In: Enna SJ, Bylund DB, editors. *xPharm: the comprehensive pharmacology reference*. New York: Elsevier; 2007. p. 1–4.
- [35] Montecucco A, Zanetta F, Biamonti G. Molecular mechanisms of etoposide. *Excli j* 2015;14:95–108.
- [36] Temaj G, Chichiarelli S, Eufemi M, Altieri F, Hadziselimovic R, Farooqi AA, et al. Ribosome-directed therapies in cancer. *Biomedicines* 2022;10(9).
- [37] Hsu EC, Shen M, Aslan M, Liu S, Kumar M, Garcia-Marques F, et al. MCM2-7 complex is a novel druggable target for neuroendocrine prostate cancer. *Sci Rep* 2021;11(1):13305.
- [38] Chan NT, Huang J, Ma G, Zeng H, Donahue K, Wang Y, et al. The transcriptional elongation factor CTR9 demarcates PRC2-mediated H3K27me3 domains by altering PRC2 subtype equilibrium. *Nucleic Acids Res* 2022;50(4):1969–92.
- [39] Sadeghi L, Prasad P, Ekwall K, Cohen A, Svensson JP. The Paf1 complex factors Leo1 and Paf1 promote local histone turnover to modulate chromatin states in fission yeast. *EMBO Rep* 2015;16(12):1673–87.
- [40] Wood S, Willbanks A, Cheng JX. The role of RNA modifications and RNA-modifying proteins in cancer therapy and drug resistance. *Curr Cancer Drug Targets* 2021;21(4):326–52.
- [41] Dörner K, Ruggeri C, Zemp I, Kutay U. Ribosome biogenesis factors—from names to functions. *EMBO J* 2023;42(7):e112699.
- [42] Gujral P, Mahajan V, Lissaman AC, Ponnampalam AP. Histone acetylation and the role of histone deacetylases in normal cyclic endometrium. *Reprod Biol Endocrinol* 2020;18(1):84.
- [43] van Wijnen AJ, Bagheri L, Badreldin AA, Larson AN, Dudakov A, Thaler R, et al. Biological functions of chromobox (CBX) proteins in stem cell self-renewal, lineage-commitment, cancer and development. *Bone* 2021;143:115659.
- [44] Ma X, Kang S. Functional implications of DNA methylation in adipose biology. *Diabetes* 2019;68(5):871–8.
- [45] Wang Z, Zang C, Cui K, Schones DE, Barski A, Peng W, et al. Genome-wide mapping of HATs and HDACs reveals distinct functions in active and inactive genes. *Cell* 2009;138(5):1019–31.
- [46] Behera J, Kelly KE, Voor MJ, Metreveli N, Tyagi SC, Tyagi N. Hydrogen sulfide promotes bone homeostasis by balancing inflammatory cytokine signaling in CBS-deficient mice through an epigenetic mechanism. *Sci Rep* 2018;8(1):15226.

- [47] Wang TY, Chang MM, Li YJ, Huang TC, Chien S, Wu CC. Maintenance of HDACs and H3K9me3 prevents arterial flow-induced venous endothelial damage. *Front Cell Dev Biol* 2021;9:642150.
- [48] Lin K, Wei L, Wang R, Li L, Song S, Wang F, et al. Disrupted methionine cycle triggers muscle atrophy in cancer cachexia through epigenetic regulation of REDD1. *Cell Metab* 2025;37(2):460–476.e468.
- [49] McLean CY, Bristol D, Hiller M, Clarke SL, Schaar BT, Lowe CB, et al. GREAT improves functional interpretation of cis-regulatory regions. *Nat Biotechnol* 2010;28(5):495–501.
- [50] Ge SX, Jung D, Yao R. ShinyGO: a graphical gene-set enrichment tool for animals and plants. *Bioinformatics* 2020;36(8):2628–9.
- [51] Alvarez-Guaita A, Patel S, Lim K, Haider A, Dong L, Conway OJ, et al. Phenotypic characterization of Adig null mice suggests roles for adipogenin in the regulation of fat mass accrual and leptin secretion. *Cell Rep* 2021;34(10):108810.
- [52] Zhang L, Zhao Y, Ning Y, Wang H, Zan L. Ectopic expression of FABP4 gene can induce bovine muscle-derived stem cells adipogenesis. *Biochem Biophys Res Commun* 2017;482(2):352–8.
- [53] Ikeda Y, Tsuchiya H, Hama S, Kajimoto K, Kogure K. Resistin affects lipid metabolism during adipocyte maturation of 3T3-L1 cells. *FEBS J* 2013;280(22):5884–95.
- [54] Huang K, Jia Z, Li H, Peng Y, Chen X, Luo N, et al. Proto-oncogene FAM83A contributes to casein kinase 1-mediated mitochondrial maintenance and white adipocyte differentiation. *J Biol Chem* 2022;298(10):102339.
- [55] Freytag SO, Paielli DL, Gilbert JD. Ectopic expression of the CCAAT/enhancer-binding protein alpha promotes the adipogenic program in a variety of mouse fibroblastic cells. *Genes Dev* 1994;8(14):1654–63.
- [56] Wu Z, Xie Y, Bucher NL, Farmer SR. Conditional ectopic expression of C/EBP beta in NIH-3T3 cells induces PPAR gamma and stimulates adipogenesis. *Genes Dev* 1995;9(19):2350–63.
- [57] Holter MM, Phuong DJ, Lee I, Saikia M, Weikert L, Fountain S, et al. 14-3-3-zeta mediates GLP-1 receptor agonist action to alter α cell proglucagon processing. *Sci Adv* 2022;8(29):eabn3773.
- [58] Luo TH, Zhao Y, Li G, Zhang HL, Li WY, Ldu M. [Identification of genes that are differentially expressed in omental fat of normal weight subjects, obese subjects and obese diabetic patients]. *Zhongguo Ying Yong Sheng Li Xue Za Zhi* 2007;23(2):229–34.
- [59] Ang MY, Takeuchi F, Kato N. Deciphering the genetic landscape of obesity: a data-driven approach to identifying plausible causal genes and therapeutic targets. *J Hum Genet* 2023;68(12):823–33.
- [60] Bosi E, Marselli L, De Luca C, Suleiman M, Tesi M, Ibberson M, et al. Integration of single-cell datasets reveals novel transcriptomic signatures of β -cells in human type 2 diabetes. *NAR Genom Bioinform* 2020;2(4).
- [61] Chen S, Wasserman DH, MacKintosh C, Sakamoto K. Mice with AS160/TBC1D4-Thr649Ala knockin mutation are glucose intolerant with reduced insulin sensitivity and altered GLUT4 trafficking. *Cell Metab* 2011;13(1):68–79.
- [62] Frøsig C, Pehmøller C, Birk JB, Richter EA, Wojtaszewski JF. Exercise-induced TBC1D1 Ser237 phosphorylation and 14-3-3 protein binding capacity in human skeletal muscle. *J Physiol* 2010;588(Pt 22):4539–48.
- [63] Durcin M, Fleury A, Taillebois E, Hilairet G, Krupova Z, Henry C, et al. Characterisation of adipocyte-derived extracellular vesicle subtypes identifies distinct protein and lipid signatures for large and small extracellular vesicles. *J Extracell Vesicles* 2017;6(1):1305677.
- [64] Funcke JB, Scherer PE. Beyond adiponectin and leptin: adipose tissue-derived mediators of inter-organ communication. *J Lipid Res* 2019;60(10):1648–84.
- [65] Yin S, Liu W, Ji C, Zhu Y, Shan Y, Zhou Z, et al. hucMSC-sEVs-Derived 14-3-3 ζ serves as a bridge between YAP and autophagy in diabetic kidney disease. *Oxid Med Cell Longev* 2022;2022:3281896.
- [66] Yang Q, Loureiro ZY, Desai A, DeSouza T, Li K, Wang H, et al. Regulation of lipolysis by 14-3-3 proteins on human adipocyte lipid droplets. *PNAS Nexus* 2023;2(12):pgad420.
- [67] Kawai T, Autieri MV, Scalia R. Adipose tissue inflammation and metabolic dysfunction in obesity. *Am J Physiol Cell Physiol* 2021;320(3):C375–91.
- [68] Hinte LC, Castellano-Castillo D, Ghosh A, Melrose K, Gasser E, Noé F, et al. Adipose tissue retains an epigenetic memory of obesity after weight loss. *Nature* 2024;636(8042):457–65.
- [69] Somsen BA, Sijbesma E, Leysen S, Honzejkova K, Visser EJ, Cossar PJ, et al. Molecular basis and dual ligand regulation of tetrameric estrogen receptor α /14-3-3 ζ protein complex. *J Biol Chem* 2023;299(7):104855.
- [70] De Vries-van Leeuwen IJ, da Costa Pereira D, Flach KD, Piersma SR, Haase C, Bier D, et al. Interaction of 14-3-3 proteins with the estrogen receptor alpha F domain provides a drug target interface. *Proc Natl Acad Sci U S A* 2013;110(22):8894–9.
- [71] Saavedra-Peña RDM, Taylor N, Flannery C, Rodeheffer MS. Estradiol cycling drives female obesogenic adipocyte hyperplasia. *Cell Rep* 2023;42(4):112390.
- [72] Li R, Bernau K, Sandbo N, Gu J, Preissl S, Sun X. Pdgfra marks a cellular lineage with distinct contributions to myofibroblasts in lung maturation and injury response. *Elife* 2018;7.
- [73] Marcelin G, Da Cunha C, Gamblin C, Suffee N, Rouault C, Leclerc A, et al. Autophagy inhibition blunts PDGFRA adipose progenitors' cell-autonomous fibrogenic response to high-fat diet. *Autophagy* 2020;16(12):2156–66.
- [74] Qu JH, Tarasov KV, Chakir K, Tarasova YS, Riordon DR, Lakatta EG. Proteomic landscape and deduced functions of the cardiac 14-3-3 protein interactome. *Cells* 2022;11(21).
- [75] Agosto LM, Mallory MJ, Ferretti MB, Blake D, Krick KS, Gazzara MR, et al. Alternative splicing of HDAC7 regulates its interaction with 14-3-3 proteins to alter histone marks and target gene expression. *Cell Rep* 2023;42(3):112273.
- [76] Gao J, Sun W, Li J, Ban H, Zhang T, Liao J, et al. Rex1BD and the 14-3-3 protein control heterochromatin organization at tandem repeats by linking RNAi and HDAC. *Proc Natl Acad Sci U S A* 2023;120(50):e2309359120.
- [77] Kuzmochka C, Abdou HS, Haché RJ, Atlas E. Inactivation of histone deacetylase 1 (HDAC1) but not HDAC2 is required for the glucocorticoid-dependent CCAAT/enhancer-binding protein α (C/EBP α) expression and preadipocyte differentiation. *Endocrinology* 2014;155(12):4762–73.
- [78] Wang X, Li N, Zheng M, Yu Y, Zhang S. Acetylation and deacetylation of histone in adipocyte differentiation and the potential significance in cancer. *Transl Oncol* 2024;39:101815.
- [79] Weems JC, Griesel BA, Olson AL. Class II histone deacetylases downregulate GLUT4 transcription in response to increased cAMP signaling in cultured adipocytes and fasting mice. *Diabetes* 2012;61(6):1404–14.
- [80] Lim J, Heo Y, Choi SS. Investigation of changes in DNA methylation associated with alterations in gene expression resulting in differences between lean and obese adipogenesis. *Genomics* 2023;115(3):110623.
- [81] Park YJ, Lee S, Lim S, Nahmgoong H, Ji Y, Huh JY, et al. DNMT1 maintains metabolic fitness of adipocytes through acting as an epigenetic safeguard of mitochondrial dynamics. *Proc Natl Acad Sci U S A* 2021;118(11).
- [82] Tovy A, Reyes JM, Zhang L, Huang YH, Rosas C, Daquinag AC, et al. Constitutive loss of DNMT3A causes morbid obesity through misregulation of adipogenesis. *Elife* 2022;11.
- [83] Castellani LW, Nguyen CN, Charugundla S, Weinstein MM, Doan CX, Blaner WS, et al. Apolipoprotein All is a regulator of very low density lipoprotein metabolism and insulin resistance. *J Biol Chem* 2008;283(17):11633–44.
- [84] Parks BW, Sallam T, Mehrabian M, Psychogios N, Hui ST, Norheim F, et al. Genetic architecture of insulin resistance in the mouse. *Cell Metab* 2015;21(2):334–47.
- [85] Langfelder P, Horvath S. Fast R functions for robust correlations and hierarchical clustering. *J Stat Softw* 2012;46(11).
- [86] Chen HC, Farese RV. Determination of adipocyte size by computer image analysis. *JLR (J Lipid Res)* 2002;43(6):986–9.
- [87] Sajic T, Ferreira Gomes CK, Gasser M, Caputo T, Bararpour N, Landaluce-turrria E, et al. SMYD3: a new regulator of adipocyte precursor proliferation at the early steps of differentiation. *Int J Obes* 2024;48(4):557–66.

- [88] Baghirova S, Hughes BG, Hendzel MJ, Schulz R. Sequential fractionation and isolation of subcellular proteins from tissue or cultured cells. *MethodsX* 2015;2: 440–5.
- [89] Buenrostro JD, Wu B, Chang HY, Greenleaf WJ. ATAC-seq: a method for assaying chromatin accessibility genome-wide. *Curr Protoc Mol Biol* 2015;109:21.29.21–21.29.29.
- [90] Batie M, Frost J, Shakir D, Rocha S. Regulation of chromatin accessibility by hypoxia and HIF. *Biochem J* 2022;479(6):767–86.
- [91] Langmead B, Salzberg SL. Fast gapped-read alignment with Bowtie 2. *Nat Methods* 2012;9(4):357–9.
- [92] Mikkelsen TS, Xu Z, Zhang X, Wang L, Gimble JM, Lander ES, et al. Comparative epigenomic analysis of murine and human adipogenesis. *Cell* 2010;143(1):156–69.
- [93] Gaspar JM. Improved peak-calling with MACS2. *bioRxiv* 2018:496521.
- [94] Liao Y, Smyth GK, Shi W. featureCounts: an efficient general purpose program for assigning sequence reads to genomic features. *Bioinformatics* 2014;30(7):923–30.
- [95] Patro R, Duggal G, Love MI, Irizarry RA, Kingsford C. Salmon provides fast and bias-aware quantification of transcript expression. *Nat Methods* 2017;14(4):417–9.
- [96] Anders S, McCarthy DJ, Chen Y, Okoniewski M, Smyth GK, Huber W, et al. Count-based differential expression analysis of RNA sequencing data using R and bioconductor. *Nat Protoc* 2013;8(9):1765–86.
- [97] Quinlan AR, Hall IM. BEDTools: a flexible suite of utilities for comparing genomic features. *Bioinformatics* 2010;26(6):841–2.
- [98] Hafemeister C, Satija R. Normalization and variance stabilization of single-cell RNA-seq data using regularized negative binomial regression. *Genome Biol* 2019;20(1):296.